Target Motion Estimation Techniques for Single-Channel SAR

Mark T. Crockett

A thesis submitted to the faculty of
Brigham Young University
in partial fulfillment of the requirements for the degree of

Master of Science

David G. Long, Chair
Neal K. Bangerter
Brian D. Jeffs

Department of Electrical and Computer Engineering

Brigham Young University

June 2014

ABSTRACT

Target Motion Estimation Techniques for Single-Channel SAR

Mark T. Crockett
Department of Electrical and Computer Engineering
Master of Science

Synthetic Aperture Radar (SAR) systems are versatile, high-resolution radar imagers useful for providing detailed intelligence, surveillance, and reconnaissance, especially when atmospheric conditions are non-ideal for optical imagers. However, moving targets in SAR images are smeared. Along-track interferometry is a commonly-used method for extracting the motion parameters of moving targets but requires a dual-aperture SAR system, which may be power- size- or cost-prohibitive. This thesis presents a method of estimating target motion parameters in single-channel SAR data given geometric target motion constraints. I test this method on both simulated and actual SAR data. This estimation method includes an initial estimate, computation of the SAR ambiguity function, and application of the target motion constraints to form a focused image of the moving target. Finally, I measure its performance by investigating the error introduced in the motion estimates.

Keywords: synthetic aperture radar (SAR), GMTI, ambiguity function, backprojection

ACKNOWLEDGMENTS

Dr. David Long, thank you for helping me achieve my research goals and showing confidence in my abilities. Thank you for all the time and effort you spent guiding my research and writing. You have been a valuable mentor to me.

Thank you to the Rocky Mountain NASA Space Grant Consortium and ARTEMIS, Inc. for providing me with financial support during my research.

To my wife Mandy, I want to thank you for your patience and support throughout my research. I appreciate that even though time tables changed during my research, you remained optimistic and you have always believed in my ability to accomplish my academic goals.

Table of Contents

List of Tables

List of Figures

Chapter 1

Introduction

1.1 Motivation

For many centuries, the outcome of wars has been decided primarily by the size of opposing military forces. But during the last century, the success of any military effort has become largely dependent on military intelligence. Surveillance can help militaries prepare for and plan attacks and counter attacks by finding weak spots to exploit in the enemy's defense, tracking enemy movement, and finding supply lines. Knowing how targets move can enhance these abilities.

Visual and optical surveillance via manned aircraft were first used in World War I and became part of common military strategy in World War II. Optical imagers can be accurate, low-cost, and provide real-time target acquisition, but they underperform in the presence of clouds, fog, or darkness. Imaging radar provides similar results but its performance is not compromised by poor atmospheric conditions. Traditional imaging radar requires a long antenna to produce a finely-spaced imaging grid, but synthetic aperture radar (SAR) utilizes radar platform motion and a small antenna to synthesize a long antenna aperture in order to produce fine-resolution images.

Similar to optical images, moving targets in SAR images are generally smeared or blurred. If the motion parameters of the target are known, this effect can be alleviated by compensating for target motion. In order to extract these motion parameters, a SAR system may employ along-track interferometry (ATI) by using two antennas separated by a baseline to form two images of the same scene at different times. The images can then be compared for phase differences on a pixel-to-pixel basis, which indicate the presence of moving targets [1].

Recent technological advancements have facilitated the development of small, low-power, low-cost SAR systems which are often found on small unmanned aircraft systems (UAS). In the last ten years, UAS have become quite common in reconnaissance because they are cost-efficient and inherently less risky than manned surveillance aircraft. UAS usually have very tight payload and power restrictions which may prohibit the use of two antennas for ATI. Since single-channel Doppler shift measurements rely on either the target or the observer being stationary, we cannot perform ATI with a single antenna. These conditions motivate us to investigate a practical method for focusing single-channel SAR images of moving targets.

1.2 Thesis Statement

Ground moving target indication (GMTI) is a radar operation mode used to discriminate targets from surrounding clutter. Previous work shows that the GMTI solution of a moving target in single-channel SAR is not unique. A complete GMTI solution for targets with uniform motion requires solving for four parameters (target position in range and azimuth, heading, and speed) but single-channel SAR data has only enough information to solve for three [2]. To address these issues, this thesis explores GMTI for constrained single-channel SAR. This thesis: (1) considers how to constrain the problem sufficiently in order to get the complete GMTI solution for a moving target in single-channel SAR; (2) examines various moving target scenarios of uniformly-moving targets in simulated and actual SAR data; (3) measures the performance of the algorithm in actual data with an error analysis of the motion estimates.

1.3 Outline

This thesis is organized as follows. Chapter 2 gives an overview of SAR, the geometry that makes it possible, its signal properties, and image processing. In Chapter 3, I discuss the behavior of moving targets in a SAR image, the non-unique nature of moving target signatures in single-channel SAR data, and a SAR moving target ambiguity function. Chapter 4 provides the base of the work in this thesis by demonstrating successful target motion parameter estimation for constant motion using simulated SAR data. In Chapter 5,

I present the algorithm used to estimate uniform motion in actual SAR data, perform several case studies on various types of uniform target motion, and present an error analysis of the algorithm. In Chapter 6, I discuss conclusions from this work and future work.

Chapter 2

Background

A critical factor in evaluating SAR performance is signal-to-noise ratio (SNR). It simply compares the received signal power to the noise power, which interferes with the signal of interest. The SNR of a SAR system can be expressed as

$$SNR = \frac{P_t G^2 \lambda^2 \sigma n_p}{(4\pi)^3 R^4 P_n} \tau \beta, \tag{2.1}$$

where P_t is the transmitted power, G is the antenna gain, λ is the carrier wavelength, σ is the radar cross-section, n_p is the number of pulses used to image a single pixel, τ is the pulse duration, β is the signal bandwidth, R is the slant range from the radar to a target, and P_n is the receiver noise power [3].

This chapter provides a background of SAR systems, including their geometry, signal properties, resolution, antenna design, target scattering properties, and image formation. Throughout this chapter, I also review all of the pertinent terms listed in Eq. (2.1), which is known as the radar range equation (RRE).

2.1 SAR Geometry

Synthetic Aperture Radar works as it does primarily because the radar is usually on a moving platform – typically an aircraft or spacecraft. SAR images can often be visualized in terms of "slow time" and "fast time." Slow time refers to an amount of time relating to the coherent processing interval whereas fast time refers to an amount of time on the order of one inter-pulse period, which is generally orders of magnitude less than the inter-pulse period. In this thesis, I use "azimuth" to reference the direction of flight (slow time, along-track direction) and "range" to reference the direction orthogonal to the azimuth direction (fast time, cross-track direction).

There are three common types of SAR operation modes: stripmap, spotlight, and scanning. In stripmap mode, the antenna pointing direction (radar line of sight (LOS)) is fixed orthogonal to the azimuth direction or squinted forward or backward. As the aircraft moves along its flight path, the antenna's footprint also moves along the ground at the same velocity. The SAR transmits and receives many pulses for the same point on the ground, but it images a "strip" of ground. In spotlight mode, the antenna moves (using a gimbal or a phased array) so that it remains pointed at the same spot on the ground throughout the data collection. This allows better SNR and resolution because of the longer dwell time on a single area. In scanning SAR, the antenna moves side-to-side in range to increase the width of the imaging swath. This thesis focuses exclusively on non-squinted stripmap SAR, as depicted in Fig. 2.1.

Several factors dictate the area of ground to be imaged. The length of time that pulses are successively transmitted and received is called the collection time and determines the length of the image. The desired imaging swath width determines the maximum pulse repetition frequency (PRF) and the unambiguous range. The PRF is given by

$$PRF = \frac{1}{PRI}, \tag{2.2}$$

where PRI is the pulse repetition interval, which is the amount of time between consecutive transmit pulses. In order to distinguish one received pulse from another, they must not overlap. Therefore, the PRF must be low enough that the echo from the farthest edge of the swath for one pulse is received before the echo from the nearest edge of the swath for the next pulse. The PRF determines the unambiguous range R_{ua}, which is given by [3]

$$R_{ua} = \frac{c}{2PRF}, \tag{2.3}$$

where c is the speed of electromagnetic wave propagation. That is, R_{ua} is the maximum range at which target echoes are received without interfering. Targets at a range greater than R_{ua} alias to an "apparent range" that is within the imaging swath. Also, since the unambiguous Doppler $f_{d_{ua}}$, or range of Doppler frequencies that can be measured without aliasing is given by [3]

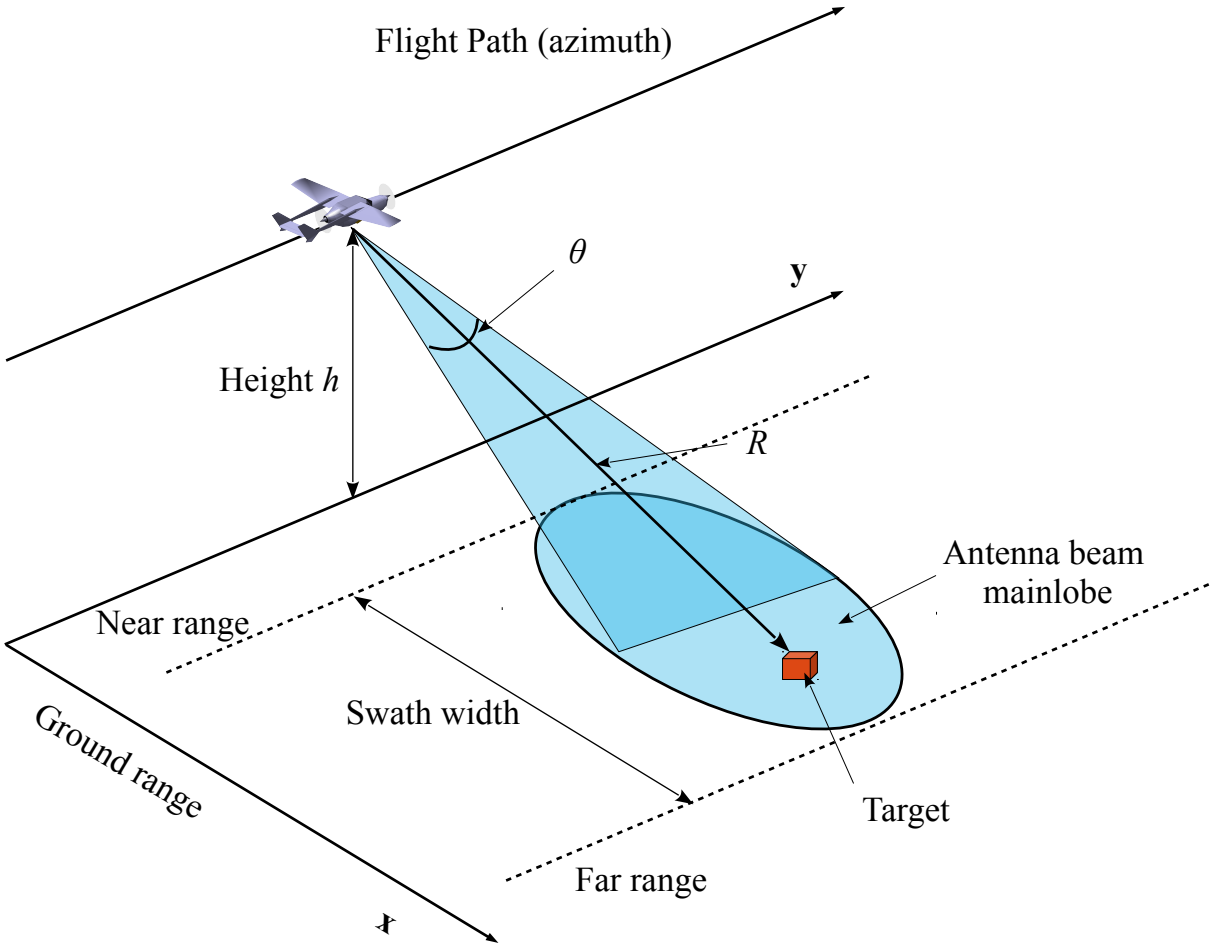

Figure 2.1: Stripmap SAR imaging geometry.

$$f_{d_{ua}} = PRF, \tag{2.4}$$

the PRF must be as large as the expected range of Doppler shifts observed by the radar. This range of observed Doppler frequencies B_d is

$$B_d = \frac{4v}{\lambda} \sin\left(\frac{\theta_3}{2}\right) \sin\psi, \tag{2.5}$$

where v is the radar platform velocity, λ is the carrier wavelength, θ_3 is the antenna's azimuth beamwidth, and ψ is the angle between the aircraft velocity vector and the radar LOS [3].

2.2 Signal Properties

Some radars use continuous-wave (CW) signals, which are pure-frequency signals that have uninterrupted transmission. An interrupted continuous-wave (ICW) signal is just a CW signal with a duty cycle less than 100%. In terms of signal transmission and reception, a SAR system works much like a traditional imaging radar. The earliest forms of SAR used ICW signals, but most now employ some type of linear frequency-modulated (LFM) signal.

Figure 2.2 shows an example of an ICW signal. It has a constant frequency and a pulse duration τ defined by

$$\tau = d_t \cdot PRI, \tag{2.6}$$

where d_t is the transmit duty cycle, or the percentage of one pulse period that the signal is transmitting.

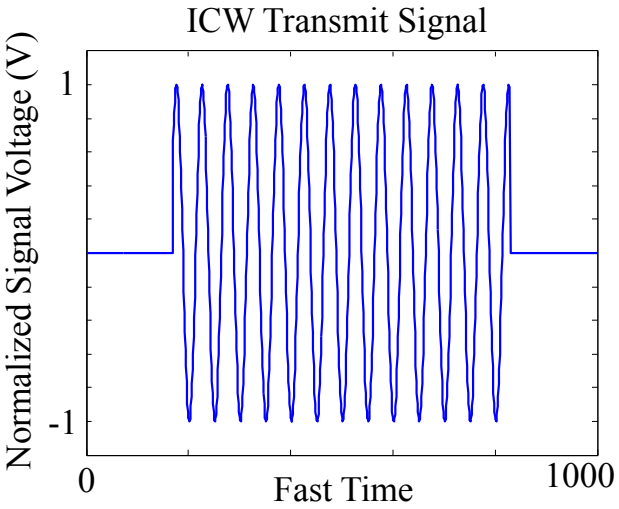

Figure 2.2: A rectangular-windowed ICW waveform.

By contrast, while an LFM signal is also pulsed, its frequency is linearly swept from low to high or vice versa at the chirp rate k_r. Figure 2.3 shows a sample LFM signal. In general, radar transmit carrier frequencies range from 300 MHz to about 300 GHz, but for convenience, Figs. 2.2 and 2.3 show signals that have been mixed to baseband. As shown

in Fig. 2.3, the signal frequency starts at zero and ramps up to a higher frequency and this pattern repeats for every transmit pulse.

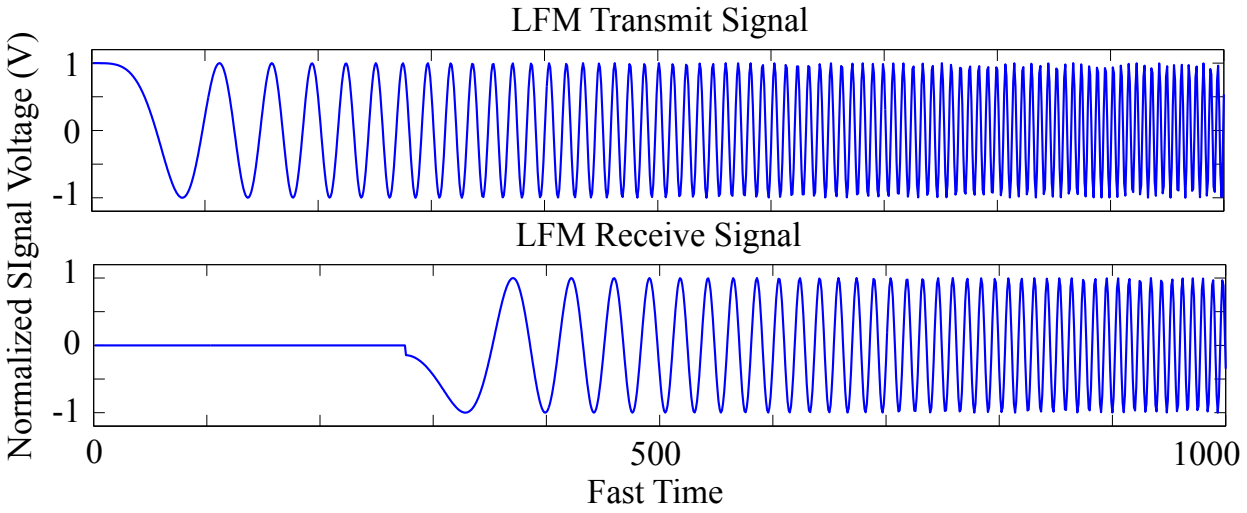

Figure 2.3: LFM transmit and receive signals.

A zero-phase LFM transmit signal $s_t(t)$ can be expressed as [4]

$$s_t(t) = A \exp\left(\jmath\left(2\pi f_0 t + \pi k_r t^2\right)\right), \tag{2.7}$$

where A is the signal amplitude at time t and f_0 is the carrier frequency. The received signal $s_r(t)$ is just an attenuated, time-shifted copy of the transmit signal and is given by

$$s_r(t) = A' \exp\left(\jmath\left(2\pi f_0 (t - \Delta t) + \pi k_r (t - \Delta t)^2\right)\right), \tag{2.8}$$

where A' is the attenuated signal amplitude and Δt is the two-way time of flight from the radar to a target at range R:

$$\Delta t = \frac{2R}{c}. \tag{2.9}$$

For convenience in processing, the received signal is usually mixed down to baseband and is given by

$$s_{rmd}(t) = A' \exp\left[\jmath\big(2\pi(f_0 - f_{md})t - 2\pi f_0 \Delta t + \pi k_r (t - \Delta t)^2\big)\right], \tag{2.10}$$

where f_{md} is the mix-down frequency.

2.3 Range and Azimuth Resolution

The effective resolution of a SAR image is defined as the half-power width of the impulse response (IPR) [5], which is a point target's appearance in the final SAR image. There are two types of spatial resolution defined for a radar imaging system: range resolution and azimuth resolution. These quantitatively define how closely targets can be spaced in each image direction and still be individually recognized by the radar.

One very common metric for range resolution is called Rayleigh resolution, which is defined as the separation between the peak and the first null of the matched filter response [3]. The Rayleigh range resolution of a pulsed waveform can be expressed as

$$\Delta x = \frac{c}{2\beta} = \frac{c\tau}{2}, \tag{2.11}$$

where β is the signal bandwidth [3]. If the distance in range between two scatterers is greater than Δx, the radar receives distinct signal returns from each and we say that the targets are resolved. If not, their signal echoes interfere with each other and cannot necessarily be accurately separated.

The Fourier uncertainty principle [6] states for a given signal that

$$\sigma_t \sigma_w \geq \frac{1}{2}, \tag{2.12}$$

where σ_t and σ_w are the standard deviations of the pulse duration and the signal bandwidth, respectively. A common interpretation of the uncertainty principle is that a signal cannot have both narrow bandwidth and short pulse duration. This provides the foundation for the relationship $\frac{1}{\beta} = \tau$ between LFM and ICW signals seen in Eq. (2.11).

Since its range resolution is directly related to pulse duration, ICW radar benefits from very short pulses (low duty cycle). However, SNR requirements necessitate more transmit power, which means transmitting a longer pulse. Since these two ICW system requirements

conflict where LFM systems do not, LFM signals are generally preferred to ICW ones. Furthermore, LFM signals can be lengthened for the sake of higher average power without degrading range resolution since it is only dependent on the range of frequencies swept by the signal chirp.

The azimuth resolution Δy of a real aperture radar imaging system is given by

$$\Delta y = \theta_3 R, \tag{2.13}$$

where θ_3 is the antenna's horizontal 3 dB beamwidth (Eq. (2.17)) and R is the slant range to the target [5]. This means that the best resolution in real aperture radars is achieved with the narrowest beamwidth (long antenna) and closest range to the target possible. These design specifications severely limit the use and performance of real aperture systems. However, Eq. (2.13) can be related to the SAR system model by substituting the synthetic aperture beamwidth for θ_3.

The synthetic aperture along-track beamwidth θ_{3s} is given by [5]

$$\theta_{3s} = \frac{\lambda\alpha}{2L_s}, \tag{2.14}$$

where L_s is the maximum length of the synthetic aperture and is equal to $\theta_3 R$. Substituting Eq. (2.14), L_s, and subsequently Eq. (2.17) into Eq. (2.13) gives

$$\Delta y_s = \theta_{3s} R = \frac{\lambda\alpha R}{2L_s} = \frac{\lambda\alpha R}{2\theta_3 R} = \frac{\lambda\alpha R}{2\frac{\lambda\alpha}{L}R}. \tag{2.15}$$

After simplifying, this equation becomes

$$\Delta y_s = \frac{L}{2}. \tag{2.16}$$

Here, we introduce one of the most important properties of SAR imaging systems: that the azimuth resolution is independent of the carrier wavelength and range to the target. Thus, we can achieve incredibly-fine resolution images just by using a smaller antenna.

2.4 Antenna Design

Part of what makes SAR so versatile is its ability to produce fine-resolution images without the use of a long antenna. In fact, many SAR systems are intentionally designed to utilize a very short antenna, but a SAR antenna that is too small suffers from degraded SNR.

According to [3], an antenna's beamwidth is inversely proportional to its size. The antenna's beamwidth is generally understood to mean the angular width of the main lobe's radiation pattern at half power as shown in Fig. 2.4. This is often referred to as the 3 dB beamwidth θ_3 and is given by

$$\theta_3 = \frac{\lambda\alpha}{L}\text{radians}, \tag{2.17}$$

where α is a constant factor dependent on the antenna's physical properties and L is the length of the antenna. According to Eq. (2.17), the smaller the antenna, the larger the beamwidth.

SAR systems often use an antenna with a wide beamwidth in order to maximize the amount of time a target spends in the antenna's beamwidth. This is called the dwell time, and in SAR it is often used interchangeably with the coherent processing interval (CPI). Traditionally, the CPI is the number of pulses used for target detection but in SAR, the CPI or dwell time T_d is the time spent imaging a single pixel, given by [3]

$$T_d = \text{dwell time} = n_p \cdot PRI. \tag{2.18}$$

The CPI is generally equivalent to the time required for the radar platform to cover the length of the synthetic aperture.

One metric used to characterize an antenna's performance is directivity. An antenna's directivity is defined as the ratio of radiation intensity in a reference direction to the average radiation intensity [8]. The reference direction is usually in the direction of maximum radiation. Essentially, it tells us where the antenna concentrates transmitted and received power. Directivity D is directly related to the physical size of the antenna A and is given by [8]

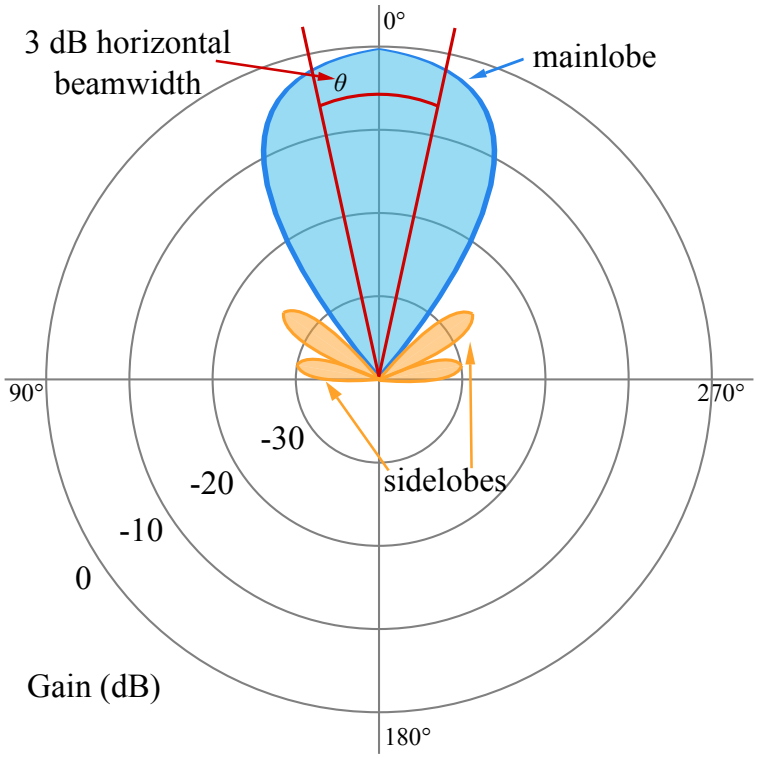

Figure 2.4: Typical antenna radiation pattern. Copyright Creative Commons, adapted from [7].

$$D = \frac{4\pi}{\Omega_A}, \tag{2.19}$$

where Ω_A is the beam solid angle, and is given by

$$\Omega_A = \int\int_{\text{sphere}} |F(\theta, \phi)|^2 \, d\Omega, \tag{2.20}$$

where $F(\theta, \phi)$ is the normalized electric field pattern. If all power emitted by the antenna were concentrated in a cone at the antenna's maximum radiation and constant distribution, the cone would span a solid angle Ω_A. The familiar gain term G in Eq. (2.1) is just the maximum directivity minus internal antenna losses.

2.5 Radar Cross-Section

Beyond the SAR platform itself, there are external factors that affect the received signal intensity. Most importantly, the radar cross-section (RCS) of the targets in the scene

of interest tells us how large a target appears to the radar. As opposed to physically-large objects that are easily detectable by human sight, RCS is a measure of a target's electromagnetically reflective strength [9], which depends not only on its physical size, but on its shape and material properties as well.

A point target is a target with small physical dimensions relative to the radar's imaging resolution, but some point targets can have a very high RCS. Consider, for instance, a trihedral corner reflector, as shown in Fig. 2.5. Corner reflectors are simple targets with known RCS that can be generalized as

$$\sigma = 4\pi A_{\text{eff}}^2/\lambda^2, \tag{2.21}$$

where A_{eff} is physical area of the corner reflector that participates in the multiple-bounce mechanism. The corner reflector in Fig. 2.5 has an A_{eff} of $a^2/2\sqrt{3}$ and an RCS of $\pi a^4/3\lambda^2$ [10]. In this thesis, the targets used in simulation behave similar to corner reflectors.

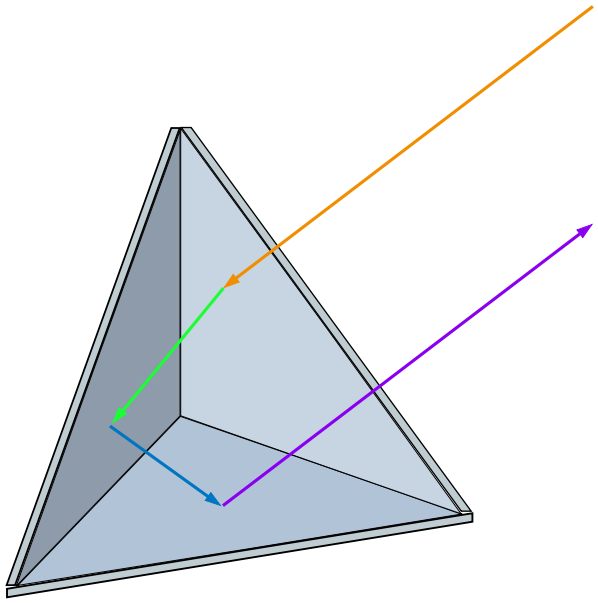

Figure 2.5: A triangular trihedral corner reflector. The design of three mutually-orthogonal sides makes this an exceptional radar imaging target. Any incident signal is reflected directly towards the source. Dihedral corner reflectors are quite prevalent in real-world data when imaging man-made structures and vehicles.

Mathematically, the RCS σ of any target can be expressed as

$$\sigma = \lim_{R \to \infty} 4\pi R^2 \frac{\left|\mathbf{E}^{scat}\right|^2}{\left|\mathbf{E}^{inc}\right|^2}, \tag{2.22}$$

where $\mathbf{E}^{scat}$ is the scattered electric field and $\mathbf{E}^{inc}$ is the electric field incident at the target [9].

2.6 Image Formation

When the radar collects data, it is stored as samples of signal amplitude and phase. We must compress the data in both range and azimuth and compensate for range cell migration in order to form an image out of it.

The most common SAR processing algorithms are the range Doppler algorithm (RDA–frequency domain), the chirp scaling algorithm (CSA–frequency domain), the omega-K algorithm (ωKA–2-D frequency domain), and the backprojection algorithm (time domain). Each of these algorithms has processing shortcomings that are briefly explained in this section.

RDA is the most commonly-used SAR processing method because it has simple implementation and is efficient and relatively accurate. However, it requires computationally-expensive interpolation to correct range cell migration. CSA was developed as an alternative to RDA and uses a more efficient method of range cell migration correction. In order to optimize processing, both RDA and CSA discard higher-order terms of the Taylor series approximation of the SAR signal and are therefore unable to accurately process wide-beam SAR data [11]. While the omega-K algorithm (ωKA) does not make SAR signal model approximations, it assumes constant radar platform velocity, which introduces errors resulting from non-linearities in the aircraft's flight path.

Backprojection is a time-domain azimuth compression algorithm that is computationally expensive but exact. Because backprojection makes no approximations it circumvents problems from SAR geometry that are common in frequency-domain methods, including wide antenna beamwidths and non-linearities in the aircraft's flight path [4]. Backprojection is the most computationally expensive algorithm of those discussed here, but recent developments in GPU computing has almost entirely removed its computational cost. My thesis deals exclusively with the backprojection algorithm.

In general, range compression and backprojection are applied to SAR data under the assumption that the either the radar platform or the targets are stationary. For pulsed SAR, a good approximation of platform motion is the stop and hop approximation. This means that the aircraft is assumed to be stationary between transmit and receive pulses. With small PRFs or very long pulse durations this approximation can cause phase estimation errors and image anomalies, but it is a reasonable approximation for pulsed SAR since the movement of the platform from pulse to pulse is negligible compared to the range to the target [12].

2.6.1 Range Compression

The matched filter is the optimal linear filter for maximizing SNR of a signal. It requires a received signal and a reference signal. The reference signal is used to extract target features in the imaging scene by measuring differences between it and the received signal. To perform range compression, the matched filter is implemented by applying an FFT to each radar echo, performing a complex multiply between the echo and the complex conjugate of the reference signal, and applying an IFFT to the product. In other words, it is a cross-correlation between transmitted and received signals. Fig. 2.6 depicts a simple diagram of how to implement range compression in SAR.

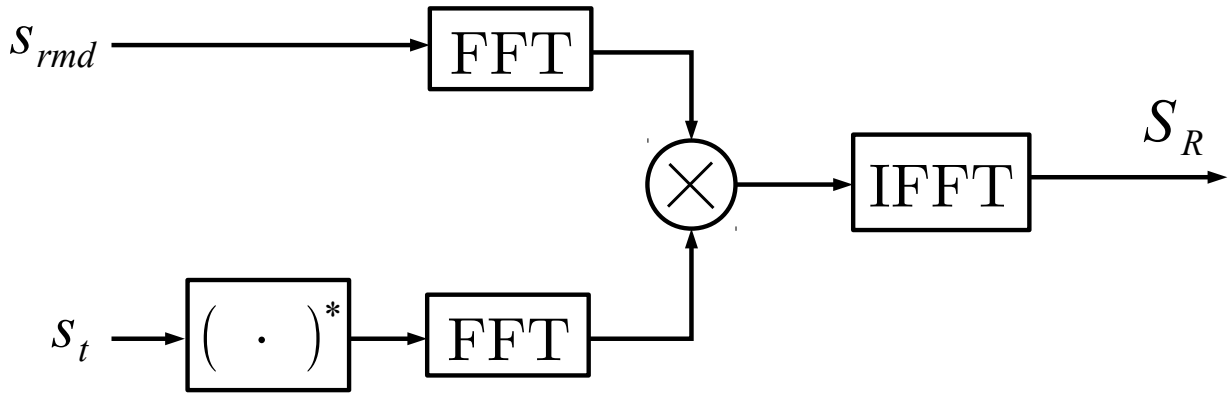

Figure 2.6: Block diagram showing the steps of range compression.

As the name implies, range compression compresses SAR data in fast time and gives a one dimensional view of the target scene for any one position in slow time. This is done for every pulse in the data collection, at which point we can perform azimuth compression. Range-compressed data is depicted in Fig. 2.7, where the range to the target varies hyperbolically, as indicated by the shape of the range migration curve.

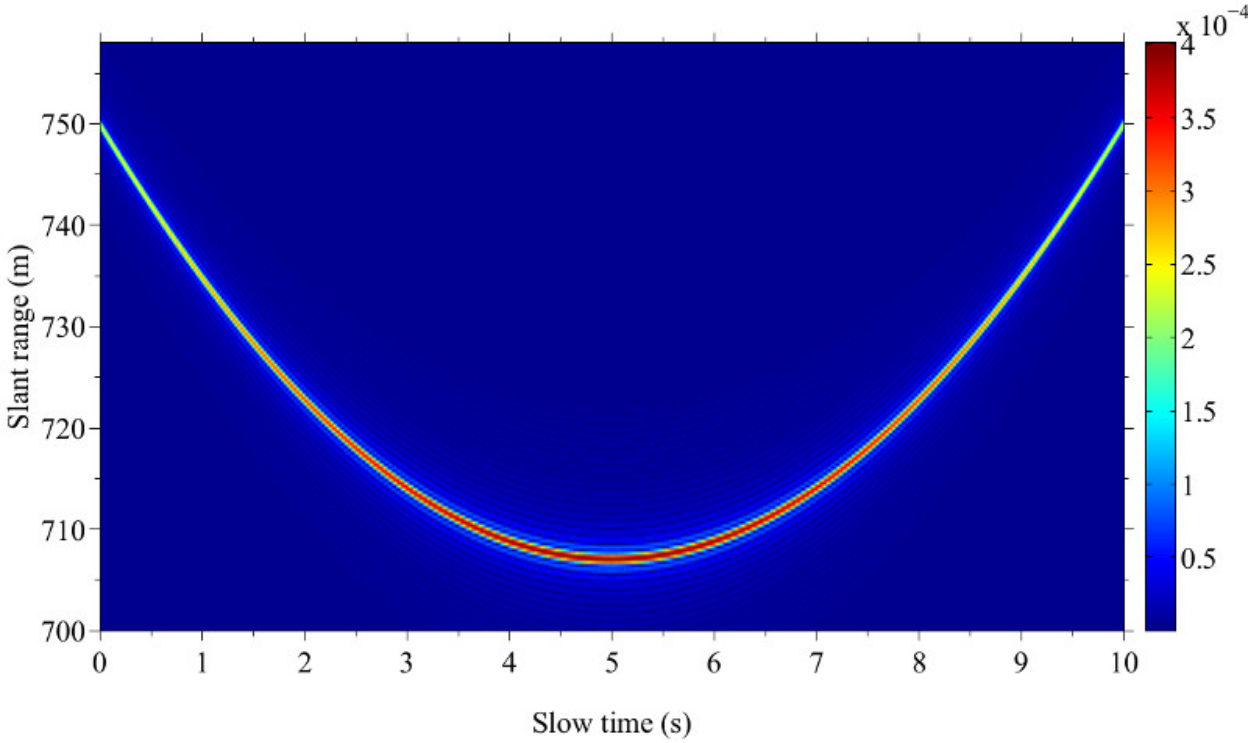

Figure 2.7: Range-compressed data for a stationary target 500 meters away from the flight path for a radar platform altitude of 500 meters. Image courtesy Joe Winkler [2]. Used with permission.

2.6.2 Range Cell Migration Correction

With wide antenna beamwidths, the dwell time on a particular pixel can be long enough that the range to that pixel changes more than one range resolution cell Δx throughout the collection. Since all the data across the synthetic aperture is used to form the final SAR image, the target appears to move through multiple range bins, which is called range cell migration (RCM). RCM complicates image focusing and in general, must be compen-

sated for to produce a focused image. Each SAR processing algorithm approaches range cell migration correction in a different way. For example, the range-Doppler algorithm (RDA) corrects for RCM by applying a frequency-dependent azimuth interpolation to straighten each pixel trajectory so its energy lies in one range bin. On the other hand, the chirp scaling algorithm (CSA) compensates for RCM without interpolation by using chirp scaling functions [12].

2.6.3 Azimuth Compression

Azimuth compression is vital to SAR because it coherently sums the data from many positions along a flight path in order to form the synthetic aperture previously discussed. Backprojection is a time-domain azimuth compression algorithm that can compensate for any beamwidth, frequency, or platform motion because it makes no signal, range, or motion approximations. Backprojection uses a matched filter for every pixel in the image by summing the product of the range-compressed data and the complex conjugate of the expected phase. The backprojection equation is given by

$$A(x,y,z) = \sum_{n}^{N} S_R\left(R[x,y,z,n]\right) \cdot \exp\left(\jmath 4\pi R\left[x,y,z,n\right]/\lambda\right), \tag{2.23}$$

where $A(x,y,z)$ is the complex pixel value at a particular location and S_R is the range-compressed data for a particular range $R[x,y,z,n]$ that has been interpolated to the range of the current pixel. The expected phase of $R[x,y,z,n]$ is $\exp\big(-\jmath 4\pi R\left[x,y,z,n\right]/\lambda\big)$, so Eq. (2.23) is just the matched filter in slow time.

2.7 Signal-to-Clutter Ratio

While the matched filter is ideal for maximizing SNR, signal-to-clutter ratio (SCR) can be even more important for measuring SAR performance. In SAR images, clutter is the radar return from objects in the imaging scene that are not of interest [3]. As opposed to thermal noise, clutter is a kind of signal interference and is only present when a radar signal is transmitted. Clutter is often measured in terms of radar cross section σ_c as follows:

$$\sigma_c = A_c \sigma^\circ, \tag{2.24}$$

where A_c is the area of the illuminated clutter cell and σ° is the normalized radar cross-section of the clutter cell (average reflectivity per unit area) [3]. It is useful to examine SCR in terms of the radar range equation adapted for the RCS of clutter. This is done by substituting the RCS in Eq. (2.1) with the RCS of the clutter cell. In this way, all but the RCS terms cancel and we are left with the signal-to-clutter ratio:

$$SCR = \frac{\sigma}{\sigma_c}. \tag{2.25}$$

In SAR images, clutter is often present in the form of speckle. Speckle is signal interference that occurs when many individual scattering centers exist in a single resolution cell. As opposed to the point targets discussed in Section 2.5 that have individually distinguishable scatterers, speckle is considered a distributed target with random scattering mechanisms [5].

Consider, for example, a field of grass. As the aircraft moves along its flight path, the aspect angle varies between each blade of grass in a single resolution cell and changes slightly between each pulse. Each blade of grass in the resolution cell has different scattering properties that vary based on aspect angle. The radar returns resulting from the grass in this resolution cell may constructively or destructively interfere during the SAR's coherent superposition of the individual returns. For this reason, speckle often has a noise-like appearance in SAR images and introduces a graininess to the images [3, 5]. An example of speckle in a SAR image is given in Fig. 2.8.

A common goal is to distinguish targets from clutter background. The problem in this is two-fold: the probability distribution function (PDF) of the target signal must be separated sufficiently from the clutter PDF in mean and variance. Since clutter usually produces higher pixel intensities than noise, SCR can be even more important than SNR for image quality and in detecting targets.

In SAR imagery, clutter can generally be understood to mean unwanted signal that interferes with the signal of interest. When the target of interest is moving, everything but

Figure 2.8: SAR image of agricultural fields in Spanish Fork, UT. Speckle can be seen resulting from the crops. It is the noise-like interference present in the image. Image brightness has been inverted for convenience. Image courtesy Artemis, Inc.

that moving target is considered clutter, includng stationary and other moving scatterers. The following chapter discusses the behavior of moving targets in SAR images, the single-channel SAR GMTI solution, and an ambiguity function for constrained target motion.

Chapter 3

Behavior of Moving Targets in SAR Data

In effect, SAR systems, like digital cameras, take a snapshot in time of a target scene. However, unlike traditional point-and-shoot cameras, SAR systems do not capture data for a single instant in time, but over an extended period of time. In this way, they can be compared to single-lens reflex cameras with slow shutter speeds. When the shutter is left open for an extended period of time, moving targets are blurred. In a photograph of a moving subject, the longer the lens aperture is left open (shutter speed), the more out of focus the subject is, as in Fig. 3.1. The length of time that a SAR is sending and receiving pulses from a target is called the collection time. In terms of signal-to-noise ratio and image resolution, SAR images benefit most from long collection times. The collection time of a SAR is synonymous with the shutter speed of a camera when a moving target is present in the imaging scene. Hence, moving targets in SAR images are smeared more with longer collection times.

However, moving targets behave very differently in SAR images than they do in optical images. In the image shown above, the tail lights of the cars on the freeway trace out their exact path. Because SAR is a coherent imaging system, moving targets do not trace out their path in the resulting image. The level and manner of defocusing in SAR images depends on both the magnitude and direction of target motion. In general, a target that has a component of motion in the along-track direction is smeared in that direction, but cross-track target motion causes displacement in the target while preserving image focus.

The rest of the chapter is organized as follows. Section 3.1 and Section 3.2 discusses the behavior in SAR images of along- and cross-track moving targets, respectively. In Section 3.3, I present the key relevant results from Winkler's work in [2]. Finally, in Section 3.4, I

Figure 3.1: Photo of night-time traffic with 2 second exposure time. The headlights and tail-lights indicate the path of the vehicles during the time that the shutter is left open. Copyright Creative Commons [13].

present an ambiguity function that is a function of target motion parameters and an analysis of the motion parameter ambiguity in that ambiguity function.

3.1 Along-Track Target Motion

A target in a SAR image with an azimuthal component of motion smears in that direction and portrays the general motion of the target [14, 15]. Azimuth smearing results from along-track target velocity, relative radial velocity between the radar and target, and radial target acceleration [16, 17]. The radar's azimuth integration angle determines how curved the target smear is. The integration angle is the angle through which the radar moves relative to a single pixel during one coherent processing interval [2]. A SAR system's largest possible integration angle is the 3 dB antenna beamwidth θ_3 and it is common for a SAR to utilize the entire beamwidth for integration in order to realize the best possible azimuth resolution [3].

The direction of the target relative to the direction of the radar platform determines the orientation of the curve. If the target's along-track component of motion is in the same

direction as the aircraft, the hyperbolic image curve is concave out from the aircraft. If the target moves in the direction opposite of the aircraft, the image smear points concave towards the aircraft [14]. The length of the smear is proportional to along-track target speed, as shown in Fig. 3.2.

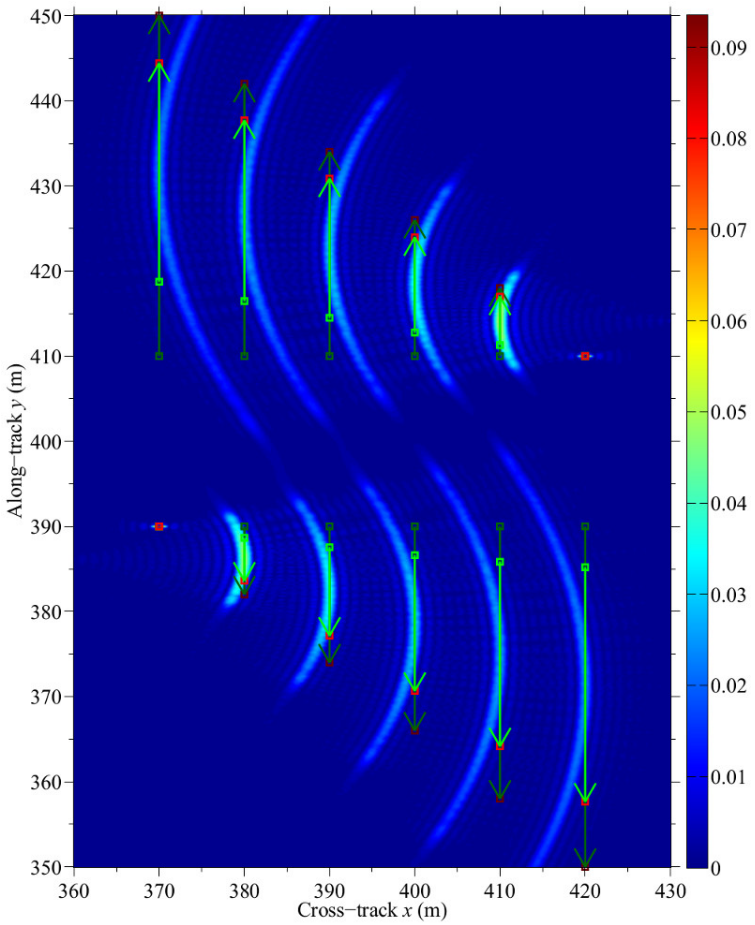

Figure 3.2: Simulated SAR image depicting the effects of along-track target motion. The radar platform is moving north at 50 m/s and looks to the right. The top six move in the same direction as the aircraft, and vice versa for the bottom six. The dark green arrows represent each target's path during the radar collection, and the light green arrow represents target motion while it is seen by the antenna. Image courtesy Joe Winkler [2]. Used with permission.

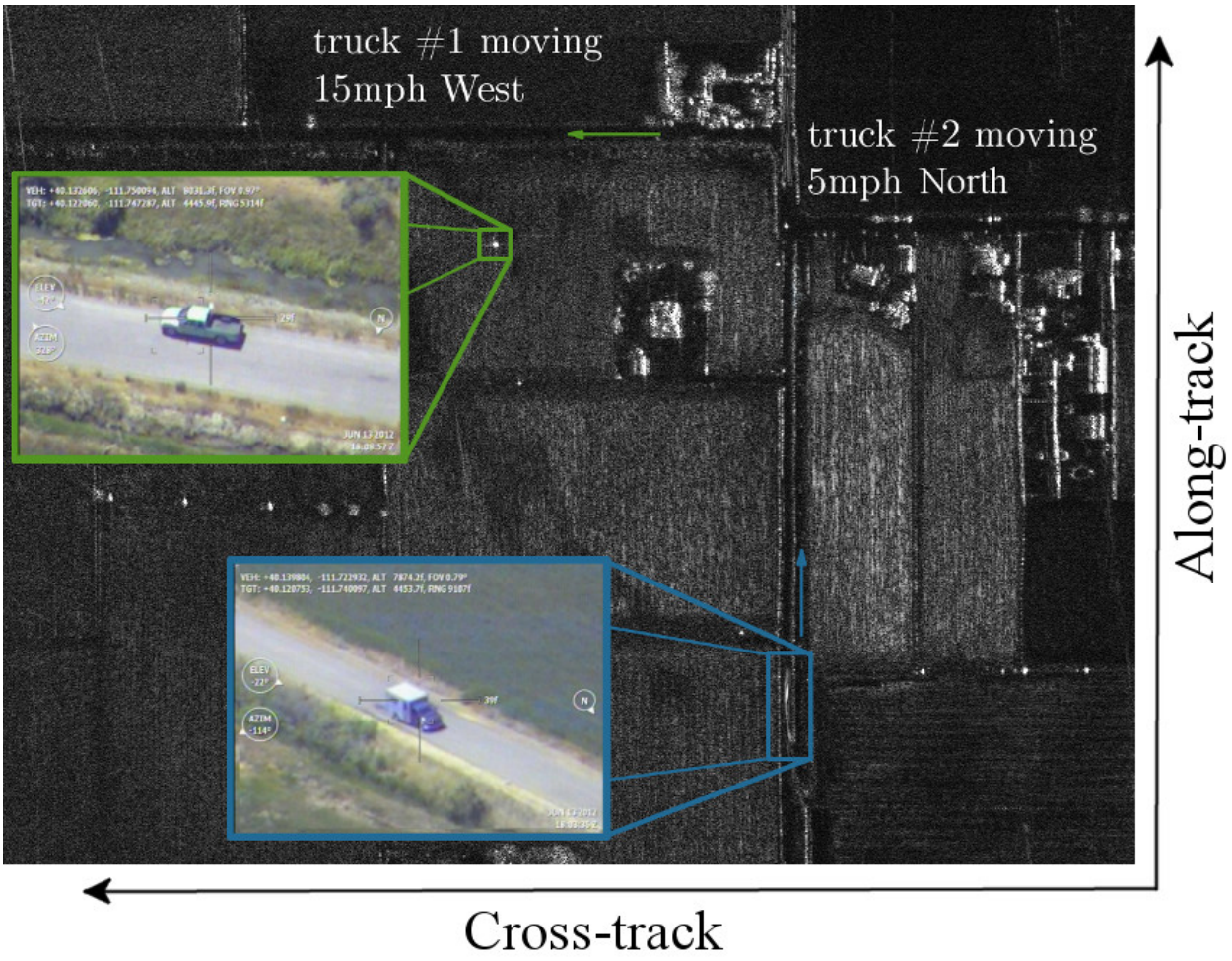

Figure 3.3: Actual SAR image of targets moving strictly in range and azimuth with optical images of vehicles overlayed on top of SAR image. The SAR platform is flying North, to the right of the image. Note that the green truck, which moves strictly in the cross-track direction, is well-focused but shifted in azimuth from the road. The blue truck, which has strictly along-track motion, is positioned correctly on the road, but is smeared in azimuth. Image courtesy Artemis, Inc.

3.2 Cross-Track Target Motion

One might expect cross-track target motion to produce a target smear in SAR images much like along-track motion does. On the contrary, cross-track motion induces much less smearing in the final target image and instead produces a shift in azimuth [14, 16, 18]. In fact, a target with strictly cross-track motion often has so little blurring that it appears as a well-focused stationary target that is shifted in azimuth from its true position. An example of cross track motion is shown in Fig. 3.3. As shown in Fig. 3.4, the true position in range

is approximately the position of the target half way through the time that it is seen by the antenna's main lobe, which is the target's position at zero Doppler shift. An image of a target that moves towards the flight path of the aircraft shifts in azimuth in the same direction as the aircraft, and vice versa for a target that moves away from the flight path.

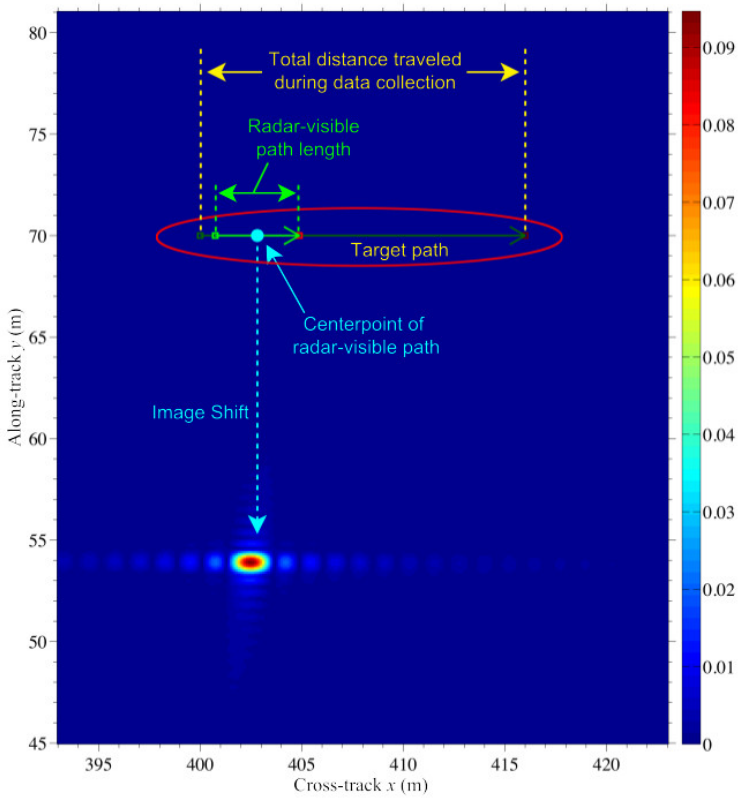

Figure 3.4: Simulated SAR image for moving target with only cross-track motion. The radar is positioned to the left of the image, looking to the right. Since the target is moving away from the radar platform, its image is shifted in the opposite direction as the aircraft. The image is shifted approximately below the position of the target when the antenna is broadside to the target, or the zero-Doppler line. Image courtesy Joe Winkler [2]. Used with permission.

The amount of shift in azimuth δx is given by [16]

$$\delta x = \frac{v_r}{v} R \bmod \theta_3 R, \tag{3.1}$$

where v_r is the target's radial velocity and v is the radar platform velocity. As we can see in Eq. (3.1), the image shift in azimuth is directly proportional to the radial velocity of the

target and range to the target and inversely proportional to the aircraft velocity. Winkler demonstrates these relationships in simulation [2], as given in Figs. 3.5 to 3.7.

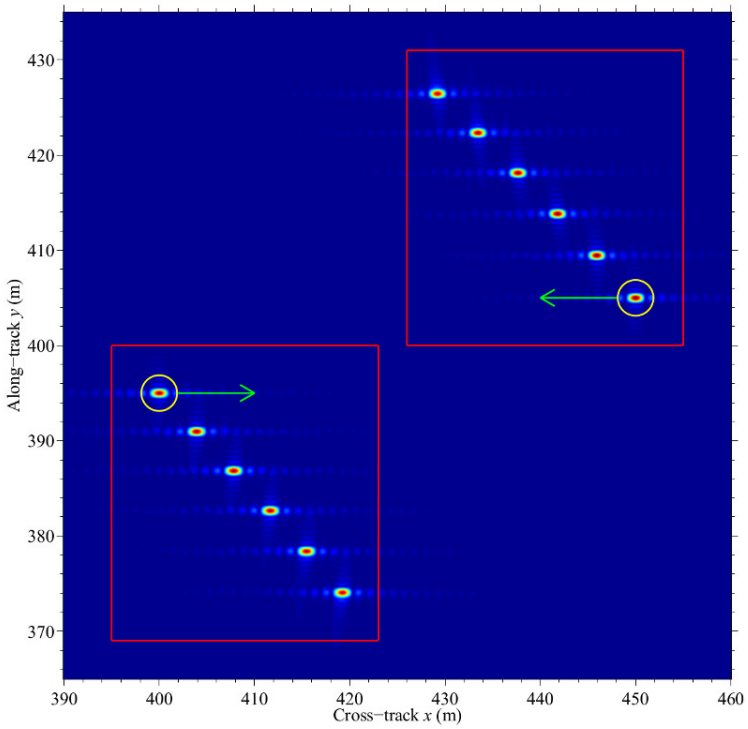

Figure 3.5: Simulated SAR images to demonstrate the direct relationship between radial velocity between the radar platform and target and amount of azimuth shift for a target moving primarily in the cross-track direction. Each target starts in the same position and moves in the direction of the green arrow with speeds ranging from 0 to 2.5 m/s in 0.5 m/s increments. Targets that move towards the flight path are shifted in azimuth the same direction as the aircraft, and vice versa for targets moving away from the flight path. Image courtesy Joe Winkler [2]. Used with permission.

3.3 GMTI for Single-Channel SAR

In general, SAR signal processing is performed under the assumption that the imaging scene contains only stationary targets. As seen in Eq. (2.23), in order to produce a fully-focused image, time-domain azimuth compression requires a phase estimate for every image pixel. In single-channel SAR, stationary targets pose no detriment to image formation since the range to an arbitrary stationary target can be known exactly using a signal's two-way

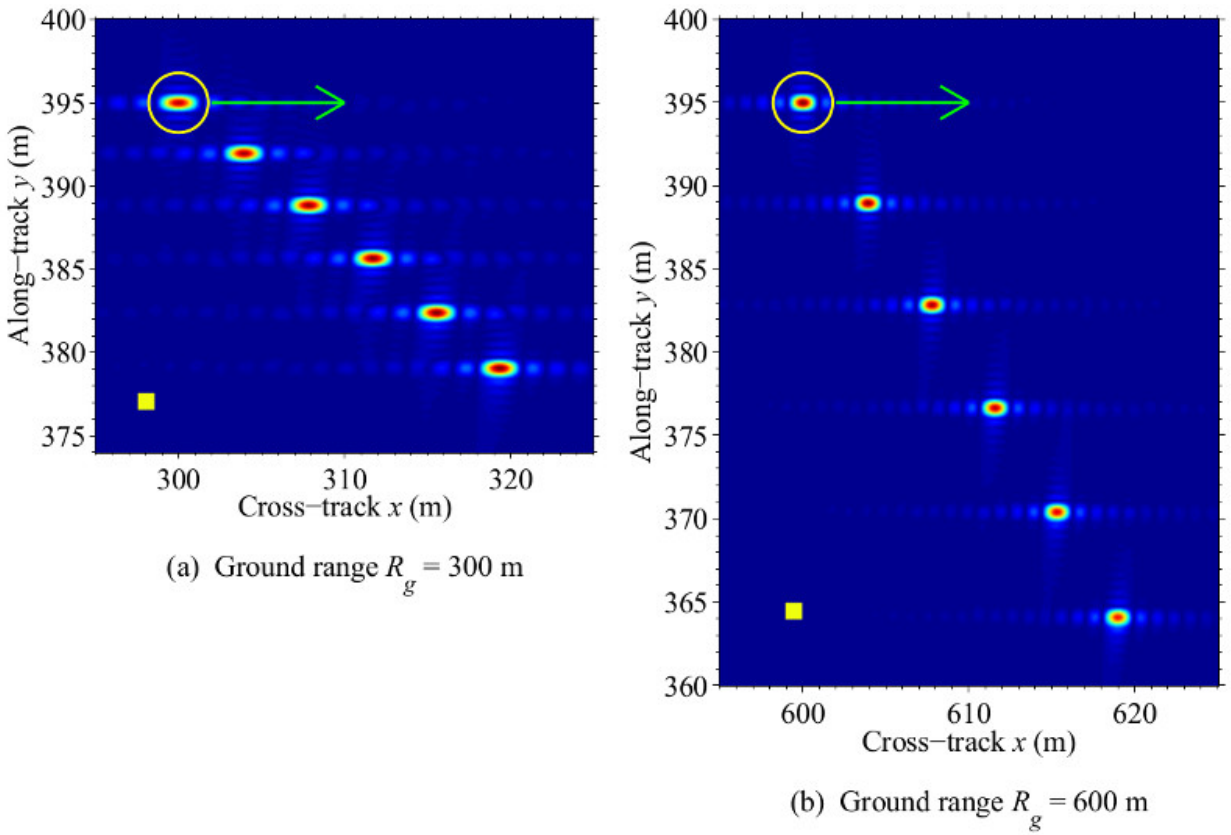

Figure 3.6: Simulated SAR images to demonstrate the direct relationship between ground range to target and amount of azimuth shift for a target moving primarily in the cross-track direction. Each target moves in the direction of the green arrow with speeds ranging from 0 to 2.5 m/s in 0.5 m/s increments. The targets in figure (b) are shifted twice as much as those in (a) because the ground range is doubled. Image courtesy Joe Winkler [2]. Used with permission.

time of flight to that target. However, the exact phase history of moving targets cannot be extracted in single-antenna SAR systems because both the moving radar platform and target contribute to phase changes of a single pixel.

Ground moving target indication (GMTI) can be performed with stationary radars by examining only radar returns with appreciable Doppler shifts. Since the radar is not moving, all stationary targets have nearly zero Doppler shift and can be ignored. The Doppler shift exhibited by any ground target is given by [3]

$$f_d = \frac{2v_r}{\lambda}, \tag{3.2}$$

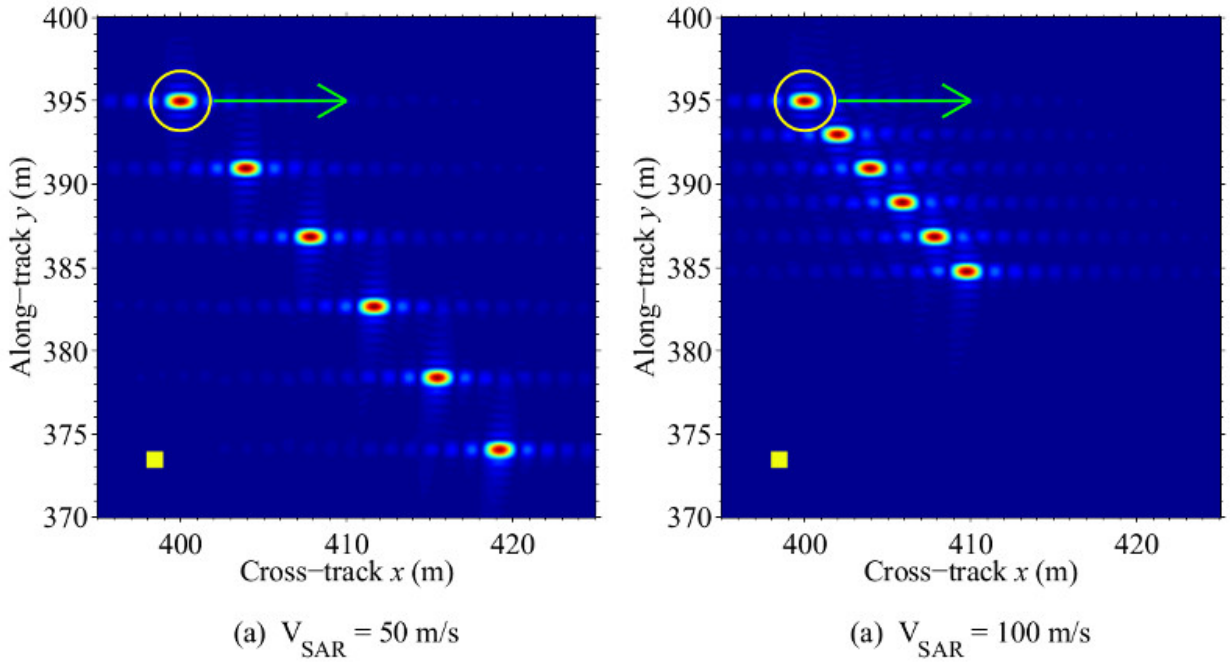

Figure 3.7: Simulated SAR images to demonstrate the inverse relationship between platform velocity and amount of azimuth shift for a target moving primarily in the cross-track direction. Each target moves in the direction of the green arrow with speeds ranging from 0 to 2.5 m/s in 0.5 m/s increments. The targets in figure (b) are shifted half as much as those in (a) because the radar platform velocity is doubled. Image courtesy Joe Winkler [2]. Used with permission.

where v_r is the radial velocity of the target relative to the radar platform. Since Doppler shift is literally a measured shift in frequency, we can extract the velocity of a moving target by measuring frequency differences between transmitted and received signals for a particular target.

However, Equation (3.2) suggests that in general, when the aircraft is moving, targets exhibit a Doppler shift. Since Doppler shift varies with relative velocity in relation to the radar, a stationary target's Doppler shift varies based on its position relative to the radar. Therefore, interfering clutter can come from many different directions and eliminating just the targets with zero Doppler shift is not sufficient in discriminating moving targets from clutter [19].

GMTI can be performed with single-channel SAR if the moving targets have a Doppler shift greater than the Doppler bandwidth of the clutter [1] as given by Eq. (2.5). However, since the clutter's Doppler bandwidth is proportional to the SAR platform velocity, slow-

moving targets cannot be extracted from the clutter because their Doppler shift falls within the clutter bandwidth.

A target's GMTI solution consists of all the parameters necessary to fully characterize the motion of the target, including but not limited to, initial position, heading, speed, and acceleration. In [2], Winkler proves that for uniform SAR platform and target motion, it is mathematically impossible to realize the target's unique GMTI solution based solely on the range migration curve (RMC), an example of which is depicted in Fig. 2.7. The GMTI solution of a target with uniform motion is given by (x_0, y_0, ψ_t, v_t), where x_0 and y_0 are the target's initial positions in range and azimuth, respectively, ψ_t is the target's heading, and v_t is the target's speed. The RMC can be expressed as a hyperbolic equation [2] in the form of

$$\frac{R^2}{\left(\frac{AC-B^2}{A}\right)} - \frac{\left(t+\frac{B}{A}\right)^2}{\left(\frac{AC-B^2}{A^2}\right)} = 1, \tag{3.3}$$

where A, B, and C are constants and are defined by the parameters of the GMTI solution. These constants are given by

$$A = v_t^2 \sin^2\psi_t + v_t^2 \cos^2\psi_t - 2v_t v \cos\psi_t + v^2, \tag{3.4}$$

$$B = x_0 v_t \sin\psi_t + y_0(v_t \cos\psi_t - v), \tag{3.5}$$

$$C = x_0^2 + y_0^2 + h^2. \tag{3.6}$$

Since all four GMTI parameters comprise the three hyperbolic function constants, the GMTI solution for single-channel SAR is an underdetermined problem. In [20], Chapman demonstrates that: 1. for every stationary scatterer, there is a set of moving targets at the same range to the radar that to the radar are indistinguishable from each other; and 2. for any moving target with uniform motion, there exists a second target with different position and velocity but same range from the target that is also indistinguishable from the first target. In single-channel SAR GMTI, this is manifest in the form of many target motion parameters that produce an identical RMC, as shown in Fig. 3.8.

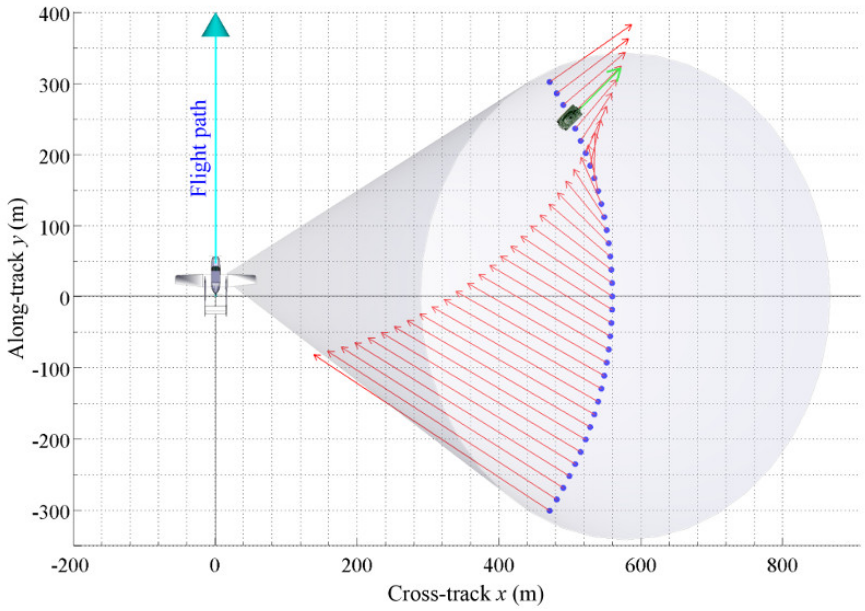

Figure 3.8: GMTI solution space for a target moving with GMTI parameters (x_0, y_0, ψ_t, v_t) of (500 m, 250 m, 45°, 10 m/s). The blue dots and corresponding red arrows represent moving target parameters that would all produce identical range history. Length of the arrows is proportional to target speed. Image courtesy Joe Winkler [2]. Used with permission.

Winkler's model, given in Eqs. (3.4) to (3.6), parameterizes a target's GMTI solution using the RMC. We can use this model to explore GMTI for single-channel SAR and it is the foundation of the new material presented in subsequent chapters.

3.4 SAR Ambiguity Function

Backprojection utilizes a 2-D matched filter to maximize image SNR. But when a moving target induces a Doppler shift in the return signal in addition to that caused by the motion of the radar platform, the return signal is mismatched to the filter and the output is lower than its maximum value. An ambiguity function (AF) is a way to characterize the response of the matched filter [3]. Examples of ambiguity functions for ICW and LFM signals are depicted in Fig. 3.9 and Fig. 3.10, respectively.

In order to show that the GMTI solution for a target with uniform motion for single-channel SAR is underdetermined, I took the following approach. Consider a single simulated SAR collection in a noise- and clutter-free environment. The only non-zero pixels in the final image come from the target's impulse response. The one target in the simulated data

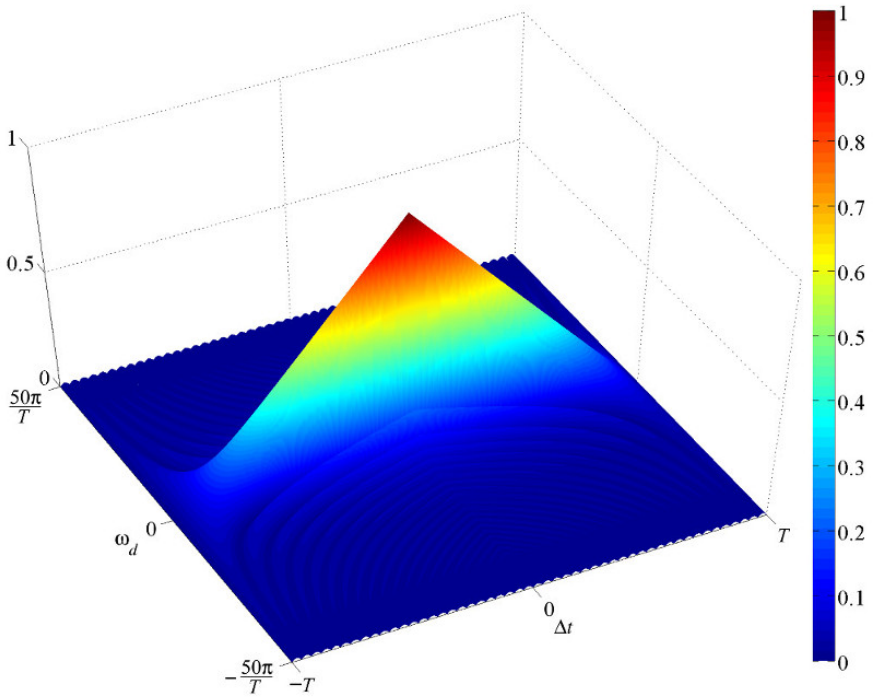

Figure 3.9: Normalized 3-D ambiguity function for a rectangular ICW pulse. ω_d is the Doppler mismatch and Δt is the time delay in the matched filter response. Image courtesy Joe Winkler [2]. Used with permission.

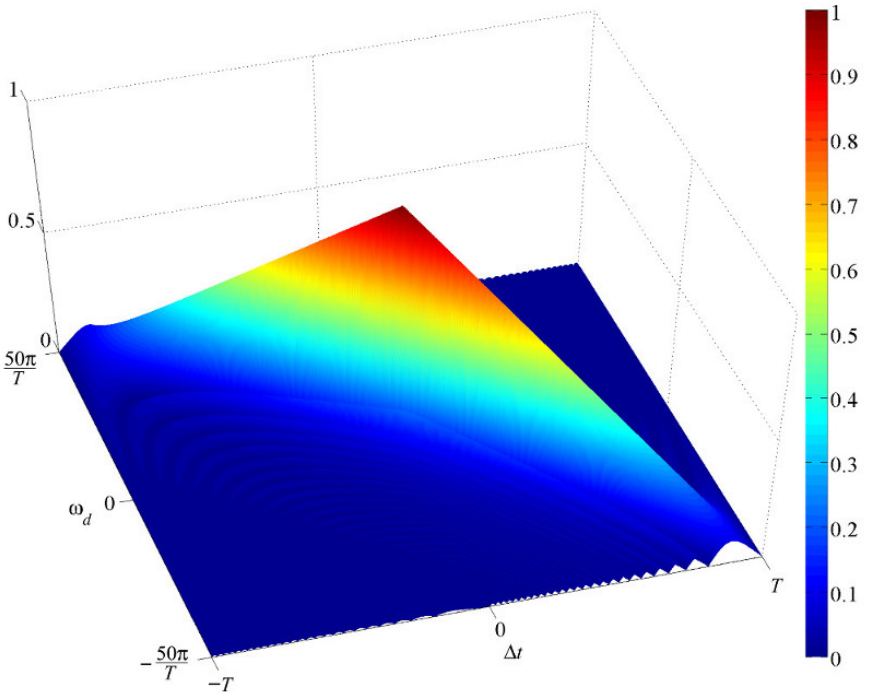

Figure 3.10: Normalized 3-D ambiguity function for an LFM pulse with a time-bandwidth product of 25. ω_d is the Doppler mismatch and Δt is the time delay in the matched filter response. Image courtesy Joe Winkler [2]. Used with permission.

is a point target and moves at a constant heading and speed. During the backprojection algorithm, the target motion can be compensated for by shifting the target pixels according to target's motion. If the wrong motion parameters are chosen, the general result is a defocused image of the target. However, suppose we process the data with motion compensation for all possible target headings and speeds to some arbitrary precision. We then have a large data set of SAR images with different levels of image focus quality. For each image, we find the largest pixel value and map that set of values on a 3-D grid with axes for the applied compensation to target heading and speed. The result can be seen in Fig. 3.11.

The conventional AF is plotted on a grid of Doppler shift and time delay [18]. However, because Fig. 3.11 depicts power as a function of parameter matching, it can be considered an ambiguity function. Since image focus and target return value are generally functions of applied motion compensation, this AF shows the most probable correct motion parameters.

The most important feature of Fig. 3.11 is the ridge that is seen near the left and right edges of the figure. I call this an ambiguity curve (AC) and give a better perspective in Fig. 3.12. These peaks in the image occur from the target return for the different focus parameters, which vary based on the accuracy of the applied motion compensation. It is important to note that in general, the true target motion parameters (15°, 10 meters/second) do not give a value any higher than the mean intensity level of the ridge[1]. In fact, each peak represents a combination of motion parameters that produce images that are virtually indistinguishable from each other and all have high target returns. As an example, consider Fig. 3.13. In this image, I have plotted 20 different combinations of motion that produce nearly identical image focus. Note that the range resolution is relatively poor relative to the azimuth resolution, so these targets are not very well focused. Also, there is slight rotation that is proportional to the error in the estimated target heading and side lobe level variation among the images, but in general, there is little to distinguish these images from each other, especially in regards to image focus.

[1]In general, tests have shown the ridge values to be similar to each other and that low peak values on the ambiguity curve result from straddle loss [3].

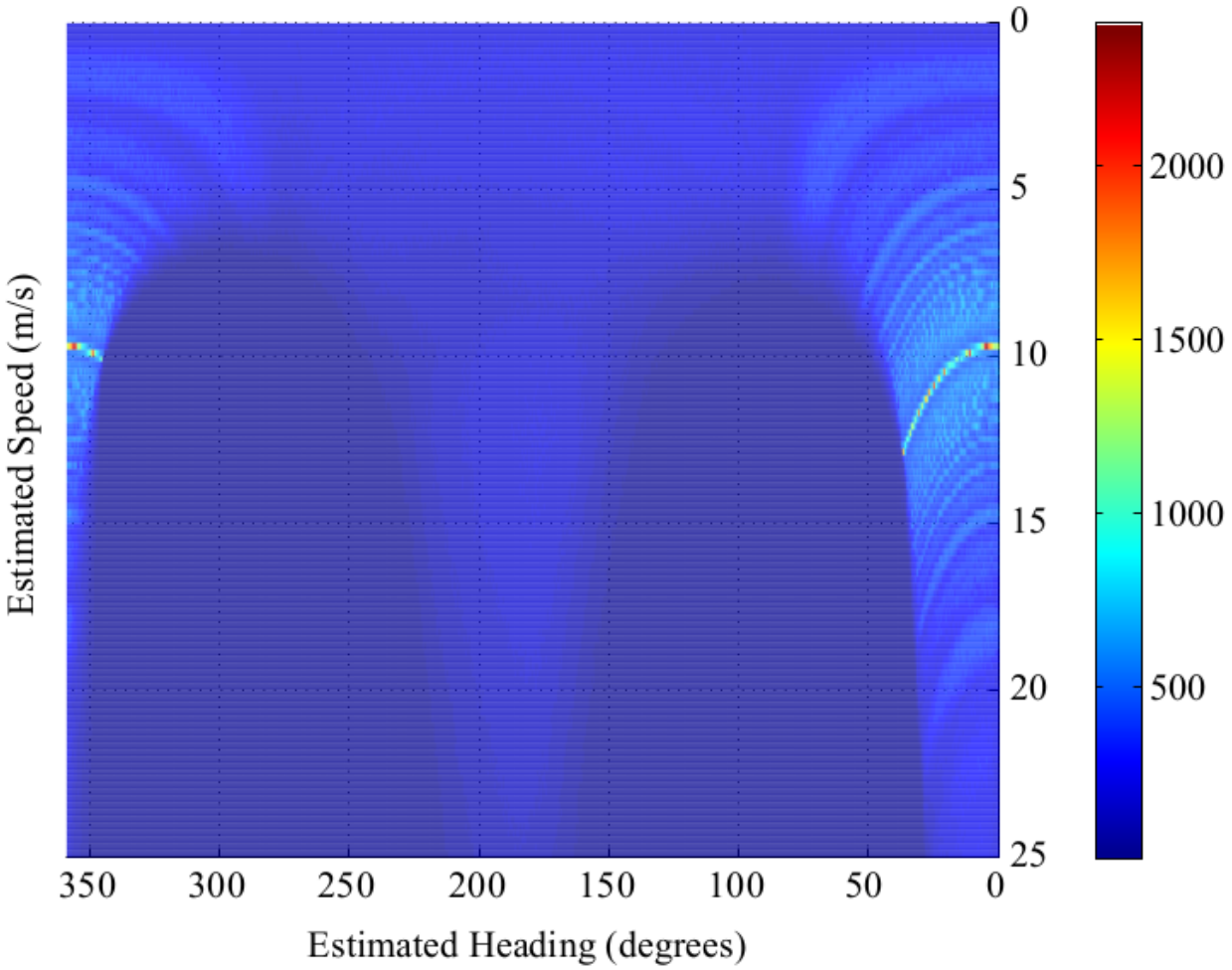

Figure 3.11: Top-down view of ambiguity function plotted for a single simulated SAR collection as a function of estimated target heading and speed. These parameters are compensated for during backprojection and each value in the ambiguity function's image is the peak pixel value for an image with some combination of target heading and speed. There is ridge of peak values starting on the left side of the image at about 10 m/s that wraps around to the right side of the image. I call this the ambiguity curve, since it represents motion parameter combinations that produce virtually indistinguishable SAR images. The two parabolic sections with zero intensity represent motion parameter compensation that caused the target to shift completely out of the imaging window.

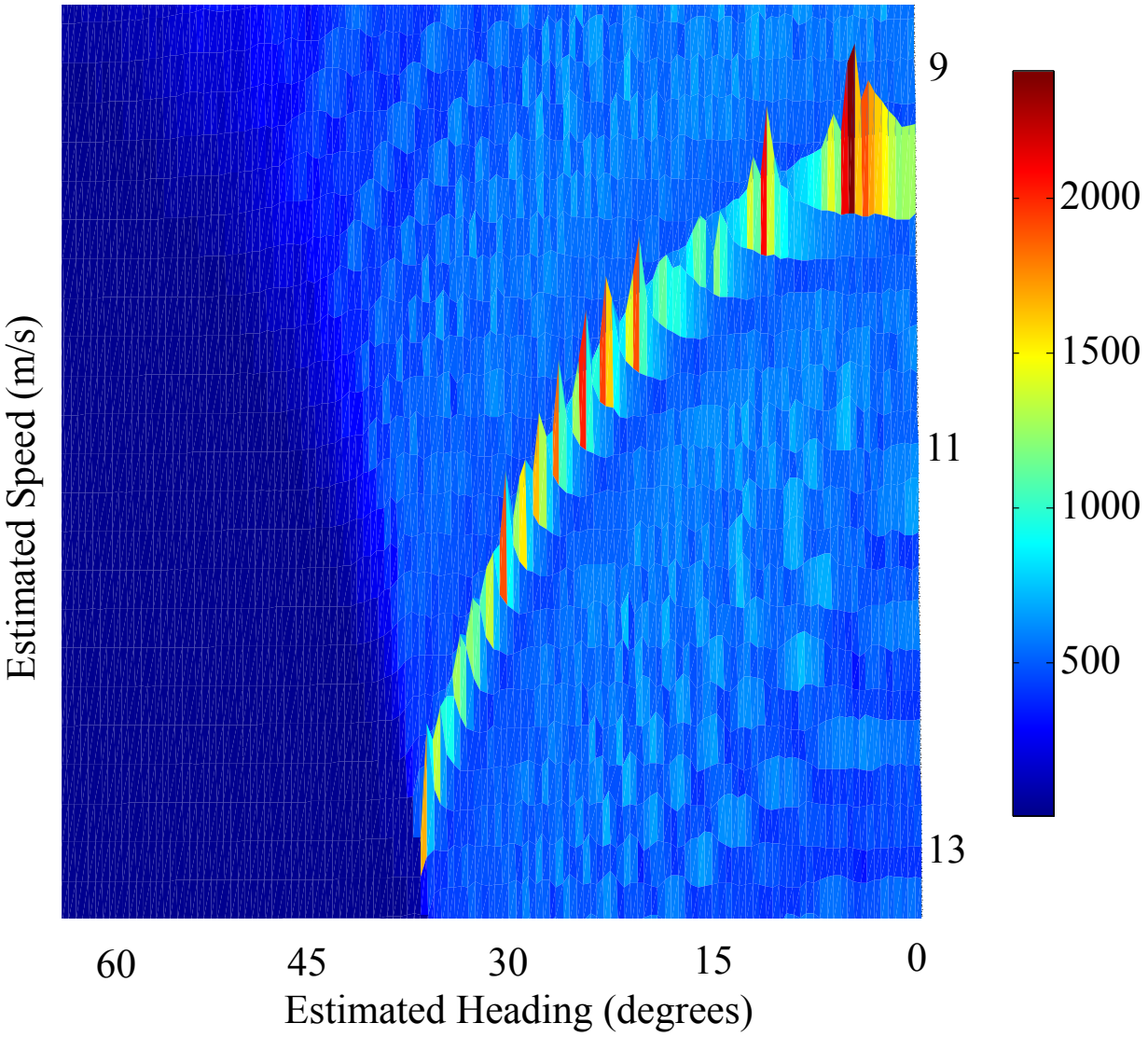

Figure 3.12: 3-D view of Fig. 3.11's ambiguity curve. The peaks of this curve represent motion parameters combinations that produce generally SAR images that are indistinguishable when applied to the same set of data.

Let us now consider image focus from a quantitative perspective. One of the most common metrics for image focus is measuring the contrast ratio of the impulse response. Contrast ratio is often defined as the ratio of the signal power in the 3 dB width of the main lobe to the power in the side lobes past the first null. I implemented this by summing the pixel intensities within the nearest 3 dB of the target center and comparing it to the side

lobe power, while ignoring a guard band from 3 dB to the first null. Table 3.1 shows a table comparing target image widths based on varying motion compensation.

Table 3.1: Mean target image widths (in pixels) in range and azimuth over all ten targets for various sets of applied motion compensation. Values here correspond to the images shown in Fig. 3.13.

3 dB (Range)	3 dB (Azimuth)	Heading	Speed
106.2	7.1	4.5	9.6
109.2	7.6	356.0	9.6
111.1	8.9	30.5	11.6
113.3	7.5	355.0	9.6
117.3	7.9	11.0	9.8
118.1	7.8	15.0	10.0
120.8	7.9	3.5	9.6
123.0	8.4	20.5	10.4
127.3	8.9	24.5	10.8
131.9	9.2	28.0	11.2
132.2	9.4	26.5	11.0
133.7	9.1	18.5	10.2
134.6	8.9	23.0	10.6
135.2	10.1	31.5	11.8
140.7	10.7	29.0	11.4
141.9	12.8	34.0	12.2
142.6	8.7	357.5	9.6
149.1	14.0	33.0	12.0
162.6	10.1	354.0	9.6
168.1	10.5	6.0	9.6

As seen in Table 3.1, there are several sets of motion parameters that produce target widths as narrow as that of the true motion parameters. This demonstrates a weakness of the implemented method of measuring contrast ratio. This weakness is manifest in the measurements of width in range and azimuth and because incorrect heading estimates rotate the final image, the measured target width for some motion parameters is less than that of the true motion parameters. Each line in Table 3.1 represents a peak in the AC shown in Fig. 3.12. As expected, each peak on the AC has an corresponding image that has similar image focus quality, as shown in Fig. 3.13.

As a matter of further investigation, let us assume that we can extract motion parameters based on image focus. Consider two SAR images from this simulated collection processed with the true motion parameters and with incorrect motion parameters providing the best quantitative image focus (4.5°, 9.6 meters/second). These are plotted side-by-side in Fig. 3.14 for comparison. They are appear nearly identical, and qualitatively, the image processed with the wrong motion parameters could be said to appear more focused than that of the true motion parameters. The only real differences are the asymmetric side lobes (left) and the rotation of the entire set of targets (right).

The preceding discussion, table, and figures demonstrate the class of moving targets described by Chapman in [20], where several combinations of target motion compensation that produce nearly identical images. This chapter has shown that the single-channel SAR GMTI solution is underdetermined. This motivates us to constrain the problem so that the GMTI solution is attainable. The next chapter demonstrates a feasible method of target motion parameter estimation if we constrain one variable of the GMTI solution.

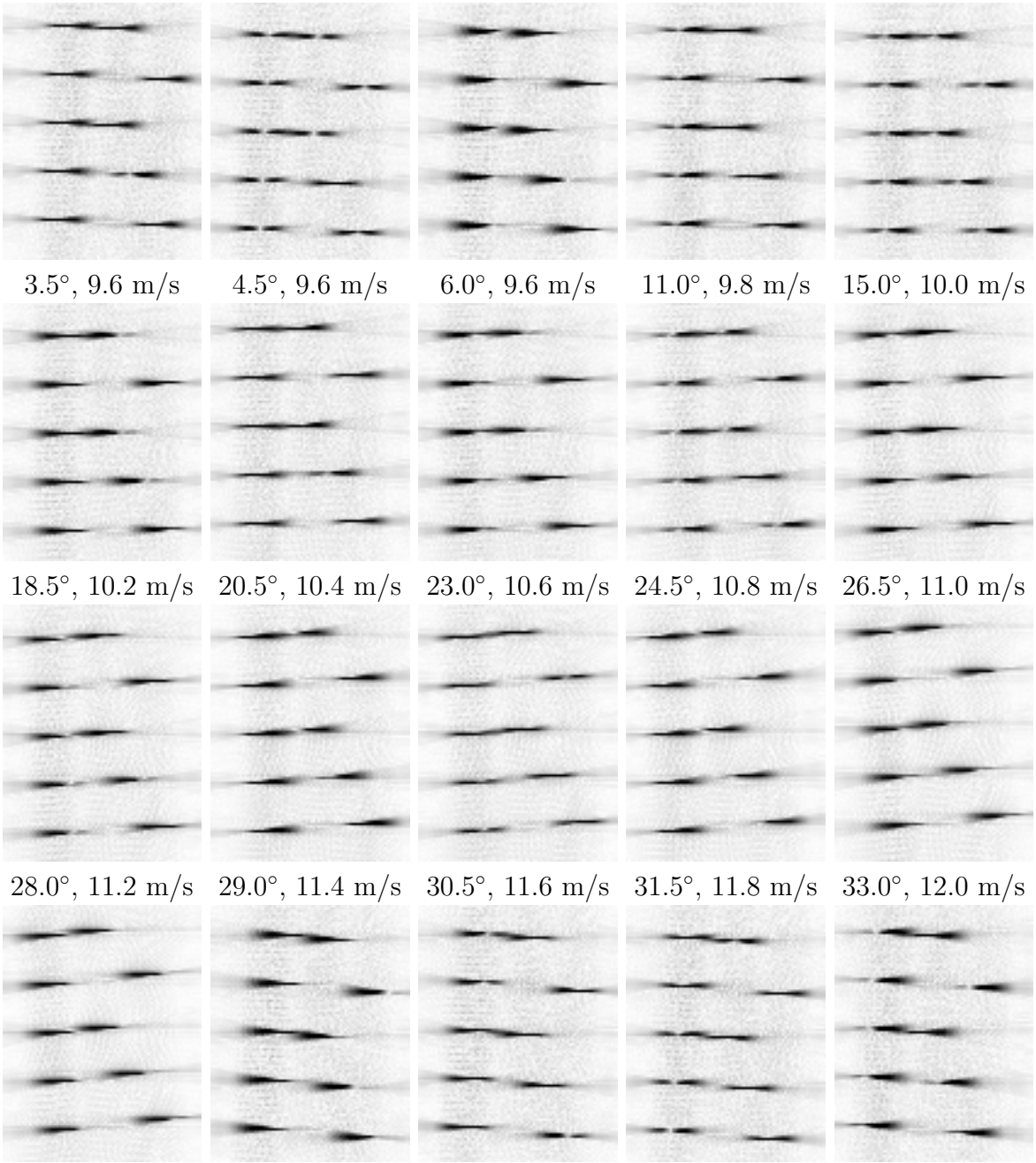

Figure 3.13: 20 SAR images processed from the same simulated SAR data with varying motion parameters. Image focus is approximately the same between all images. The motion parameters used to process each corresponding image are placed below the images. True motion parameters are 15.0°, 10.0 m/s. Image brightness has been inverted for convenience.

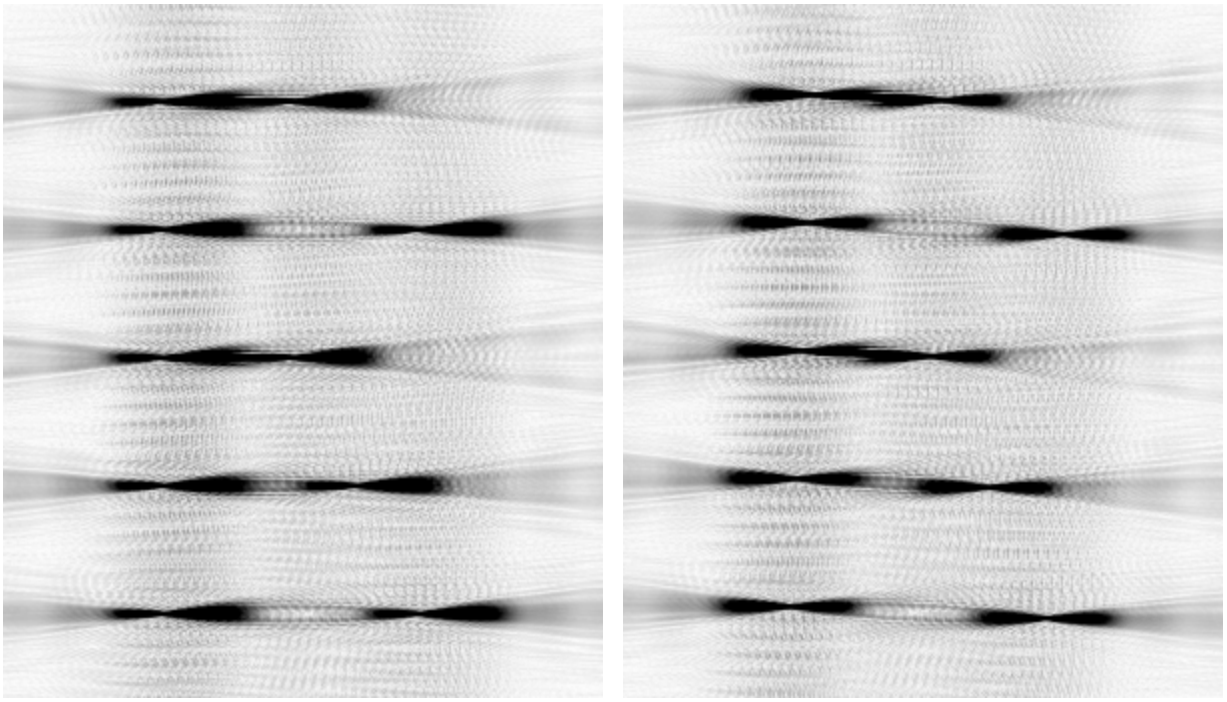

(a) 15°, 10 m/s (b) 4.5°, 9.6 m/s

Figure 3.14: Images of simulated SAR data processed with the true motion parameters (left) and incorrect motion parameters (right). Note that the images are nearly identical in image focus and intensity. Image brightness has been inverted for convenience.

Chapter 4

Estimating Target Motion Parameters in Simulated Data

We know that if a target moves uniformly, four parameters completely characterize its motion, namely position x_0 and y_0, heading ψ_t and speed v_t. Since the RMC of single-channel SAR provides only enough information to extract three of the four GMTI parameters, there are an infinite number of GMTI solutions for any given moving target in single-channel SAR. However, if we make one of the parameters a constant, it becomes possible to solve for a unique set of motion parameters using single-channel SAR data.

Considering all four motion parameters of a uniformly-moving target, the easiest parameter to constrain is heading. Since many ground targets of interest move on paved roads, for this chapter we assume that the targets of interest are traveling on straight roads which constrains the target headings to align with the road. If the target heading ψ_t is a known constant, this reduces the number of unknowns in Eqs. (3.4) to (3.6) to three. We can then solve for x_0, y_0, and v_t exactly.

In [2], Winkler approaches the GMTI problem using the range migration curve. I take a different approach in this thesis and in this chapter present a practical method of extracting the exact motion parameters using the AF shown in Fig. 3.11. This AF is in a different form than a typical AF, in that it is plotted on a grid of heading and speed as opposed to Doppler shift and time delay. However, it still indicates the level of mismatch between the return signal and the filter.

The remainder of this chapter introduces this thesis' algorithm and its application to simuated data. Section 4.1 includes a discussion of backprojection for simulated data. In Section 4.2, I give an overview of the ambiguity function formed during processing. Finally, in Section 4.3 I present some important points to consider for AF processing speed and accuracy.

4.1 Backprojection Processing of Simulated Data

Figure 4.1 shows an image of simulated SAR data. There are ten targets formed in the shape of an 'R'.

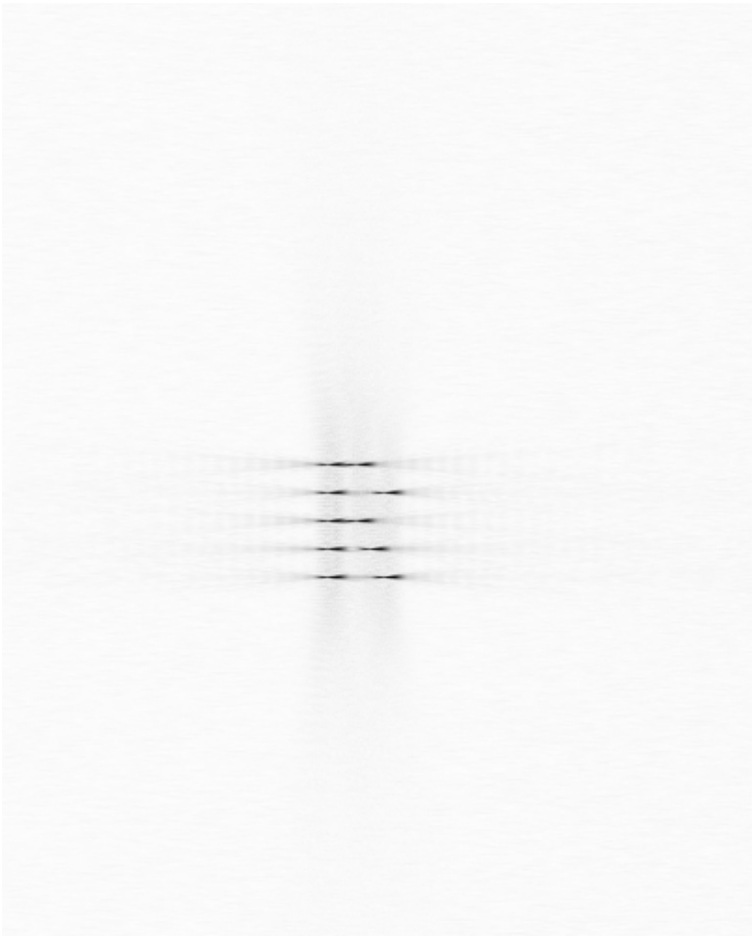

Figure 4.1: Simulated SAR image of stationary targets. Image brightness has been inverted for convenience.

Now suppose the targets move throughout the SAR collection as one rigid body at a constant velocity. In this case, the targets move with a heading of 15° at 10 m/s. This motion is constant throughout the data collection. As discussed in Chapter 3, the target smears and shifts in azimuth because of its motion as seen in Fig. 4.2.

We now have a defocused image due to motion and would like to focus it. How can we determine the correct motion parameters in order to focus the image in a reasonable

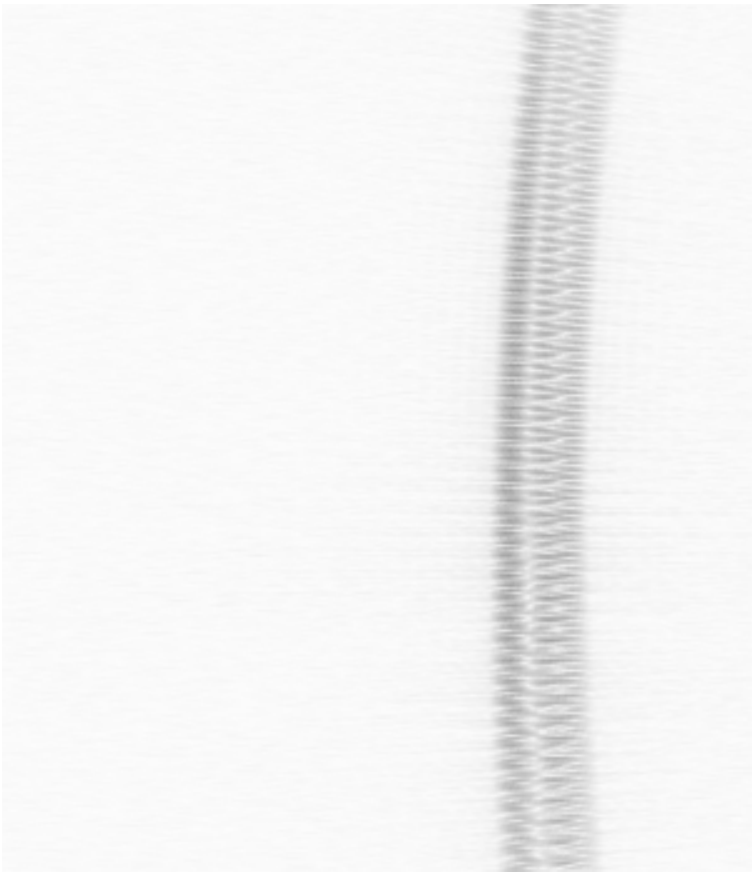

Figure 4.2: Simulated SAR image of uniformly-moving targets. Image brightness has been inverted for convenience.

amount of time? For clarity in explanation, a brief discussion of backprojection efficiency is warranted. SAR Backprojection is inherently a computationally expensive algorithm because there are $M \times N \times P$ operations to perform for every image, where $M \times N$ is the number of pixels in the image and P is the number of pulses in the data collection. A serial approach to backprojection is extremely inefficient and can take days, or even weeks for a single image. Recently, graphics card manufacturers like NVIDIA have made graphics processing units with many cores (more than 3000) on each chip [21]. Each of these chips can have hundreds of single and double precision units, special function units for trigonometric operations, and memory registers. This makes these GPUs ideal for parallel computing.

The backprojection algorithm can efficiently take advantage of all those cores and decrease the time required to process SAR data by multiple orders of magnitude [4]. All of

the SAR processing done in this thesis is performed using NVIDIA GPUs. When the task is especially computationally demanding, a high-end NVIDIA GeForce GTX 690 [21] is used.

4.2 AF Processing

Let us assume that the target of interest is moving with unknown, uniform speed but traveling on a straight road. These are reasonable assumptions for a ground-moving vehicle in any urban environment. Given this knowledge, the target heading becomes a known parameter and there are only three parameters for which to solve in the GMTI solution: position and speed. However, because it can be difficult to find the exact heading of the road and because the target heading may vary slightly from that of the road, the algorithm presented in this thesis considers a range of target headings during processing.

Since we know the general heading of the road, we need only process a section of the full AF based on a range of headings and estimated velocities, which significantly reduces the total processing time. Even a conservative estimate with large variance in target heading ($\pm$ 10°) and speed (0 – 25 m/s) reduces the processing time by a factor of twenty compared to processing the full AF from Section 3.4. The precision between heading and velocity estimates can be adjusted based on the desired AF grid spacing. Once we decide the range and precision of heading and speed estimates for motion compensation, we run backprojection on the SAR data for each combination of heading and speed, with a resulting motion-compensated image for each combination.

After backprojection processing is complete, each image is processed in MATLAB to find its maximum value, which is saved with its corresponding motion parameters. Since we are working with noise- and clutter-free simulated data, it is safe to assume that the target image contains the maximum value. The peak image pixel values are then plotted on a grid that varies with the heading and speed estimates used in processing. This is the estimated AF, an example of which is shown in Fig. 4.3.

Examining the AF, we see that there are many combinations of heading and speed estimates that give a peak in the AF. This envelope we call the ambiguity curve represents combinations of heading and speed that, when used for motion-compensation, produce target

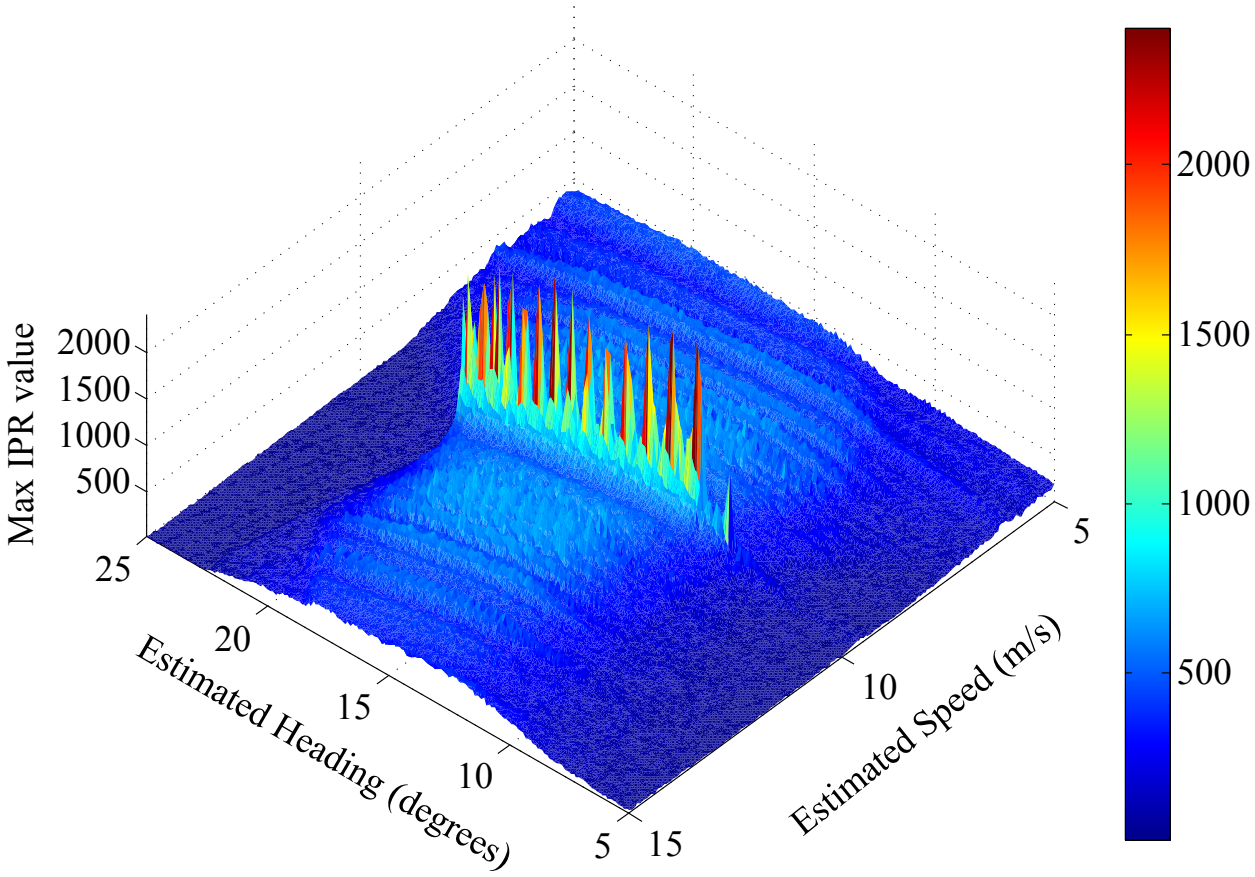

Figure 4.3: AF plotted for a target moving at 15°, 10 m/s in simulated SAR data. The AF is formed over a small heading range of for efficient processing. The peaks in the image correspond to the peaks in the ambiguity curve in Fig. 3.12.

images with similar image focus. This envelope is the source of our motion parameter estimate and is discussed in the next section.

4.3 Processing Considerations

In the first stage of processing, it is most efficient to process a coarse AF grid around the best estimates of the motion parameters in order to pinpoint a narrow range of parameters for finer processing. Examining Fig. 4.3, it is apparent that for the known target heading, target speed is fairly consistent with varying heading. This means that we can tightly constrain the range of heading estimates in our finely-spaced AF to further reduce processing time. If greater accuracy is desired or if straddle loss is encountered (Fig. 4.4), we can

decrease the AF grid size to just a few degrees in heading and a few meter/second in speed, as shown in Fig. 4.5.

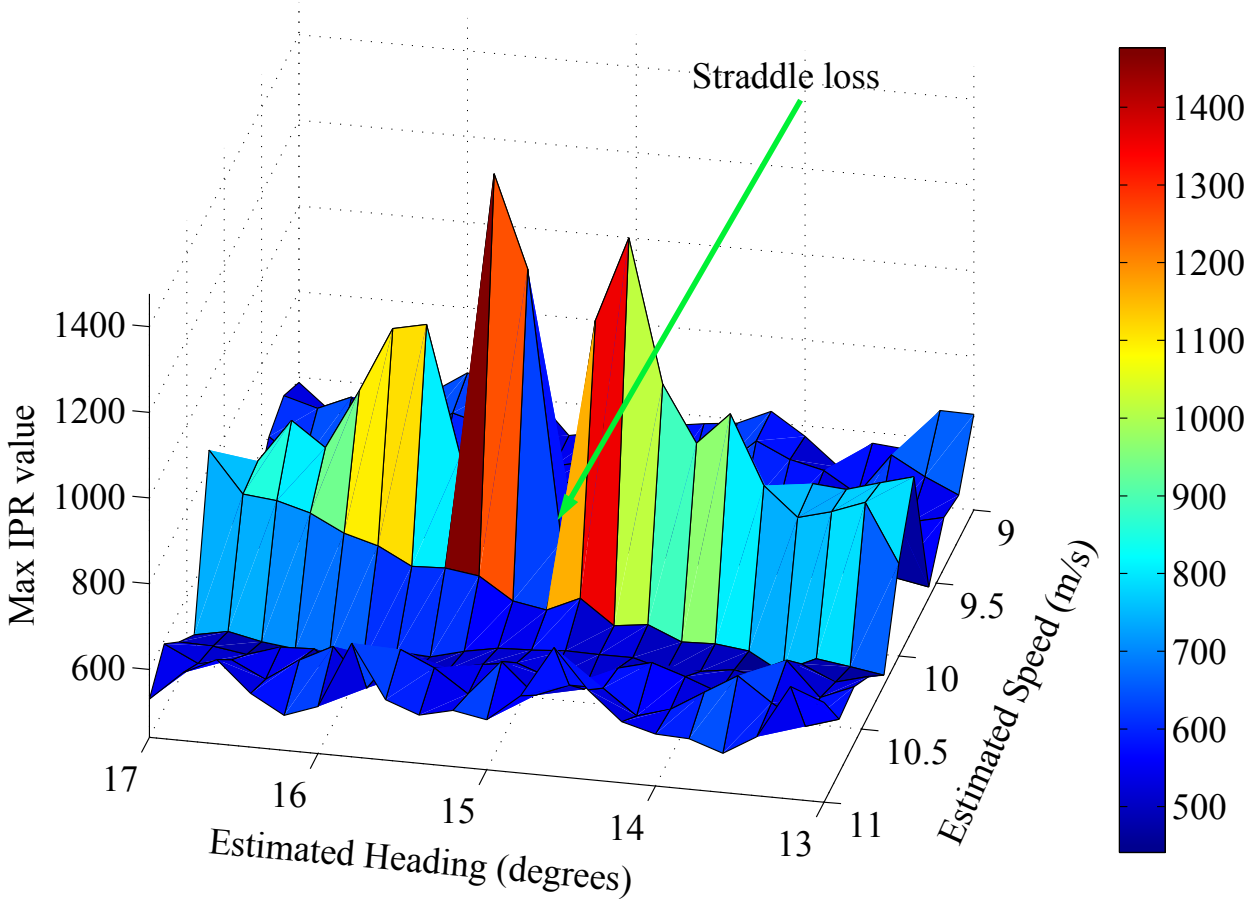

Figure 4.4: AF using coarse pixel resolution and motion parameter sampling for the same target as in Fig. 4.3. This AF suffers from straddle loss because of inadequate pixel resolution and motion parameter sampling. Pixel resolution is 10 meters and both heading and speed sample spacing is 0.2 degrees and m/s, respectively. Improving the pixel resolution gives the finer grid necessary to determine the strongest target return (and subsequently, the target motion parameters), as shown in Fig. 4.5.

In order to avoid straddle loss when forming the AF, care should be taken to use both fine-enough pixel resolution and sample spacing in the motion estimates. Straddle loss occurs when a signal is sampled infrequently enough that the signal is sampled on either side of the peak magnitude instead of at its peak [3]. Coarse pixel resolution used during backprojection may result in an image with low peak values because we are sampling on either side of a

target return instead of its peak. Likewise, if the space between motion parameter estimates is too large, we may be sampling on either side of an AF peak. Therefore, this algorithm uses finer-than-normal pixel resolution and fine motion parameter AF sampling in order to minimize straddle loss. However, if the pixel resolution or motion parameter sampling is too fine, processing the AF takes more time than is practical, so a balance must be found in the pixel sampling frequency.

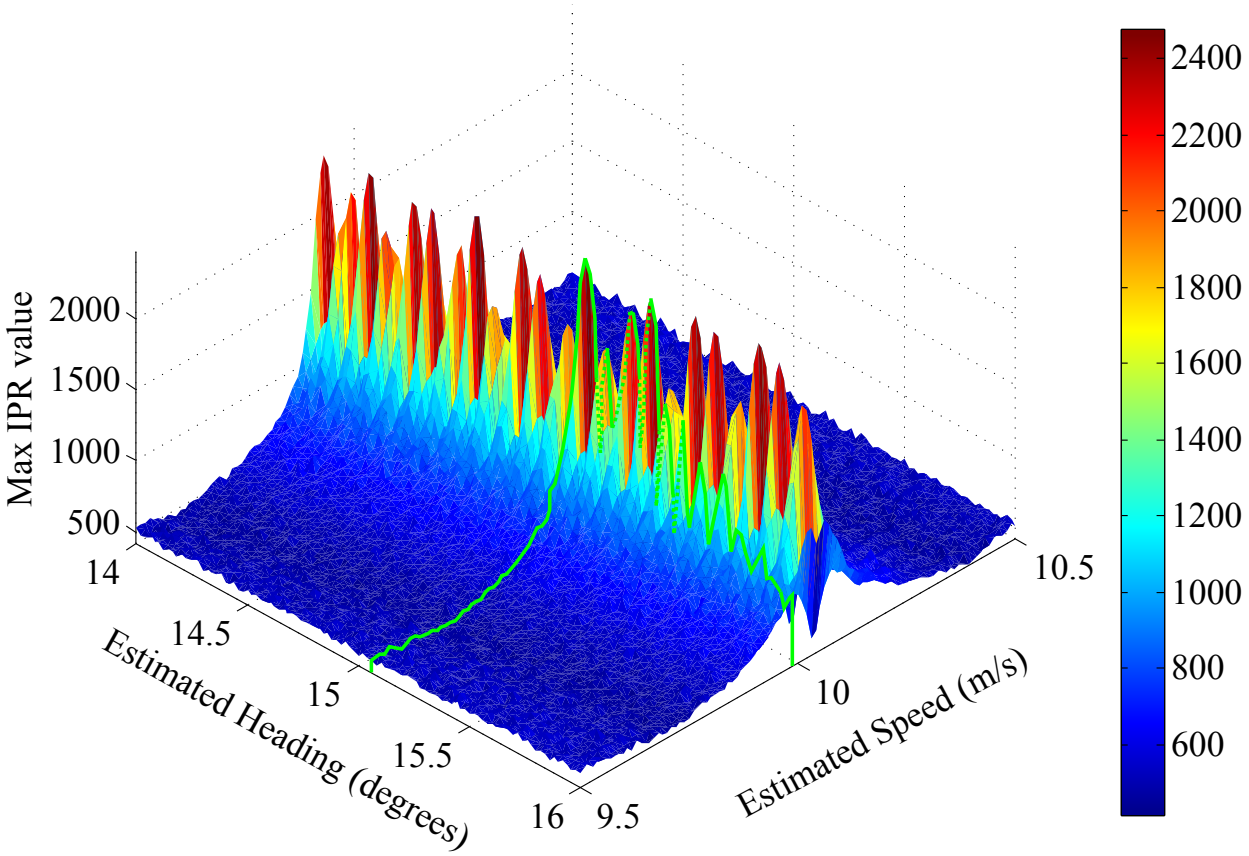

Figure 4.5: Finely-sampled ambiguity function with tighter range of heading and speed than Fig. 4.3. One line has been drawn from each motion parameter axis to the peak of the AF nearest to the known road heading. In this case, the peak is only 0.06° from the road's heading of 15°. The GMTI solution is given by the intersection of these two lines.

Although the ambiguity function in Fig. 4.5 still experiences slight straddle loss, we can still make a good estimate of target motion by searching for the peak in the envelope of the ambiguity curve. Finding the point in that envelope corresponding to the known

road heading gives us the true target motion parameters. Applying these to the SAR data introduced at the beginning of the section restores Fig. 4.2's focus and produces an image that looks identical to Fig. 4.1.

The results from the AF in Fig. 4.5 are very accurate; there is a 0.06° error in estimated heading and a 0.1% error in the speed estimate. However, this simulated SAR data is free of clutter, noise, and non-linear target and platform motion. These are all prevalent in actual SAR data and must be dealt with for this algorithm to be very useful. The following chapter adapts the algorithm as needed to make this practical for actual SAR data.

Chapter 5

Estimating Target Motion Parameters in Actual SAR Data

The previous chapter outlines a single-channel GMTI algorithm which it demonstrates with simulated data. This chapter demonstrates the algorithm with actual SAR data[1]. While the simulated data is noise- and clutter-free with idealized platform and target motion, actual SAR has significant noise, clutter, and signal phase errors introduced by non-linear platform and target motion. These negatively affect the algorithm's performance and must be dealt with.

For example, my algorithm assumes that the moving targets of interest move with uniform velocity, but since the targets are ground vehicles with human drivers, both the heading and the speed may vary during the data collection. This degrades the accuracy of the target's reported motion parameters. Non-ideal radar platform motion induces similar errors. Furthermore, the algorithm can mistake clutter for target returns, so a bounding box is set to remove clutter from the image. Lastly, some SAR data has errors that make it unusable for motion parameter estimation even though the stationary SAR image looks normal.

This chapter introduces a practical algorithm for performing single-channel SAR GMTI on actual SAR data. Section 5.1 gives a detailed description of how the algorithm is implemented for actual SAR data, including modifications required to deal with real-world problems like clutter. In Section 5.2, I demonstrate the algorithm's utility with several case studies for various types of uniform motion. Finally, Section 5.3 presents a performance analysis on the algorithm by examining the amount and sources of error in the target motion estimates.

[1]L-band SAR data and its associated truth data for target motion were provided by Artemis, Inc.

5.1 Algorithm Implementation for Actual SAR Data

The algorithm of this thesis can be divided into steps as shown in the flow chart in Fig. 5.1. These steps are outlined here and are the focus of the corresponding sections within this chapter.

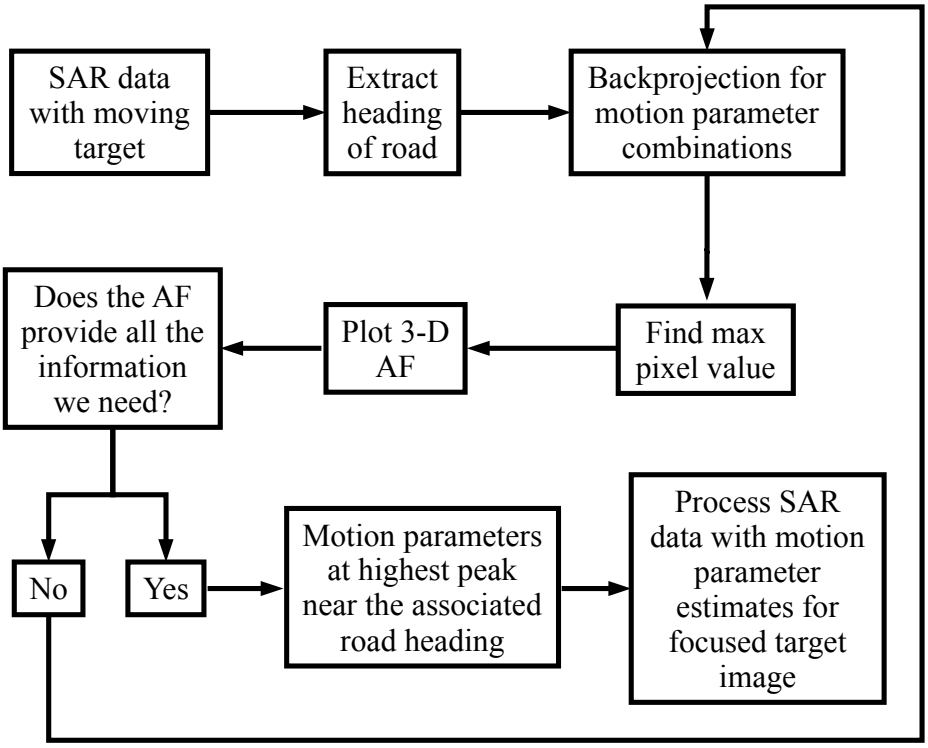

Figure 5.1: Block diagram of the single-channel SAR GMTI algorithm described in this thesis.

1. Perform backprojection processing on SAR data containing a suspected moving target without considering target motion.

2. Use shapefiles to get the heading of the road the target is traveling on.

3. Process the SAR data for a range of heading and speed estimates. For each combination of heading and speed, shift the image grid at the same rate as the estimated target motion and save an image.

4. Find the maximum image value in each motion-compensated SAR image. Ideally, this is the target's peak response.

5. Plot a 3-D ambiguity function of target values on a grid with axes associated with the range and precision of the motion estimates.

6. If necessary, process the AF again for a smaller range of motion parameter values at finer precision, centered around the peak AF values.

7. Find the highest peak in the AF at the known road heading. The heading and speed at this AF peak are our final target motion estimates.

8. Process the SAR data with the target motion estimates to generate a focused image of the moving target.

5.1.1 SAR Data with Suspected Moving Target

The first step in this algorithm is to process the SAR data containing a suspected moving target using conventional (stationary) backprojection. A moving target is smeared and/or shifted from its true position in the image. Targets with some component of along-track motion smear and are relatively easy to locate, as seen in Fig. 5.2. In this image, the target is moving at 269.7°, 11.1 m/s and because the aircraft is flying at 315°, the target has both along- and cross-track components of motion. As with all SAR images used in this chapter, the image brightness has been inverted for convenience.

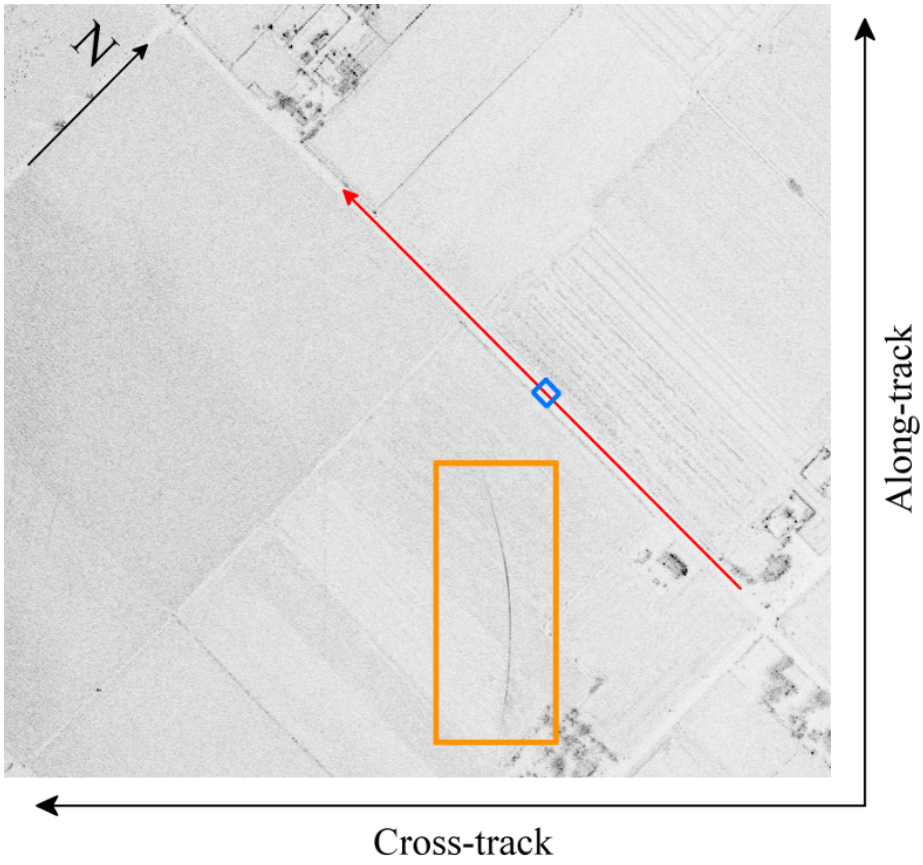

Figure 5.2: L-band SAR image of Spanish Fork, UT. The radar platform has an average heading of 315°. The target is moving at 269.7°, 11.1 m/s and can be seen as a smear in the image within the orange box. The red arrow denotes the target's path during the SAR collection and note that it is shifted from the road in the azimuth direction from it's true position, which is outlined by the blue box.

We can determine an initial estimate of the target's motion by examining the direction and magnitude of smear and shift of the target in the image. As discussed in Section 3.1, since the image smear is concave out from the radar, we know that the target's along-track component of motion is in the same direction as the radar. Likewise, we know from Section 3.2 that since the target image is shifted down from the road (opposite the direction of flight), the target's cross-track component of motion is away from the flight track. Once the target and associated road are located, the heading of the road must be determined from the orientation of the road in the image and the flight track.

5.1.2 Shapefiles

A shapefile is a common geospatial vector data format for geographic information system (GIS) software [22]. Shapefiles spatially describe a geographical area using vector features like points, lines, and polygons. Shapefiles can be used for finding the direction of roads on a map, as shown in Fig. 5.3. When shapefiles are loaded into GIS software, we can determine the exact gps coordinates of the start and end points of a road. The standard formula for bearing ψ calculated from latitude/longitude points is given by [23]

$$\psi = \text{atan2}\left[\sin(\lambda_2 - \lambda_1)\cos(\phi_2), \cos(\phi_1)\sin(\phi_2) - \sin(\phi_1)\cos(\phi_2)\cos(\lambda_2 - \lambda_1)\right], \tag{5.1}$$

where ϕ_1, λ_1, ϕ_2, λ_2 are the initial and final latitude and longitude coordinates, respectively. ψ can be normalized to a standard compass bearing by converting to degrees and adding 360° to the result. This will give us the bearing relative to 0° North. Once we have an initial heading estimate for the target's motion, which is given by the direction of the road, we can process the ambiguity function for that target's motion.

Figure 5.3: Shapefile representing the area depicted in Fig. 5.2. The roads in the image are highlighted in yellow. The red arrow indicates the target's path during the SAR collection. Since we can get the gps coordinates of the start and ending points of the target's path from the shapefile, we can easily calculate the road's heading by using Eq. (5.1).

5.1.3 AF Processing

In general, the most common SAR processing algorithm is the range-Doppler algorithm (RDA). Operating in the frequency domain, it makes some approximations of the SAR signal but is computationally efficient. These approximations are often allowable for most purposes. Backprojection is a SAR processing algorithm that, although exact in its matched filter calculations of the SAR signal and phase history, is computationally expensive. What makes backprojection so demanding is that it operates on every image pixel for each transmit pulse. With a PRF of 500 Hz this amounts to 60 billion calculations for a 4 megapixel SAR image of a 30 second SAR collection.

Fortunately, backprojection is highly parallelizable. Companies like NVIDIA have made major advances in GPU computing technology and now fit nearly 6000 processing cores

and 12 GB of memory on a single graphics card [24]. These advances, along with NVIDIA's CUDA parallel computing software, enable us to do faster-than-real-time backprojection processing.

Forming the ambiguity function used in this algorithm requires that we process a section of the SAR data up to tens of thousands of times in order to find the target's motion parameters. Therefore, we desire to minimize (1) the number of computations required and (2) the clutter present in each image. Since we are only interested in the area around the moving target, we choose an appropriate bounding box for GMTI SAR processing. For this thesis, the bounding box is generally chosen as the road the target is traveling on, as shown in Fig. 5.4. After processing the first image, which is used to determine initial target motion estimates, all subsequent images used to compute the AF are computed only within this box. This minimizes the calculations required to form the image while still giving us all the information we need to form the AF. The result is that processing time is reduced by an order of magnitude or more compared to processing the whole image. In fact, the processing takes so little time that we can greatly improve the pixel resolution of the small images without a significant increase in processing time.

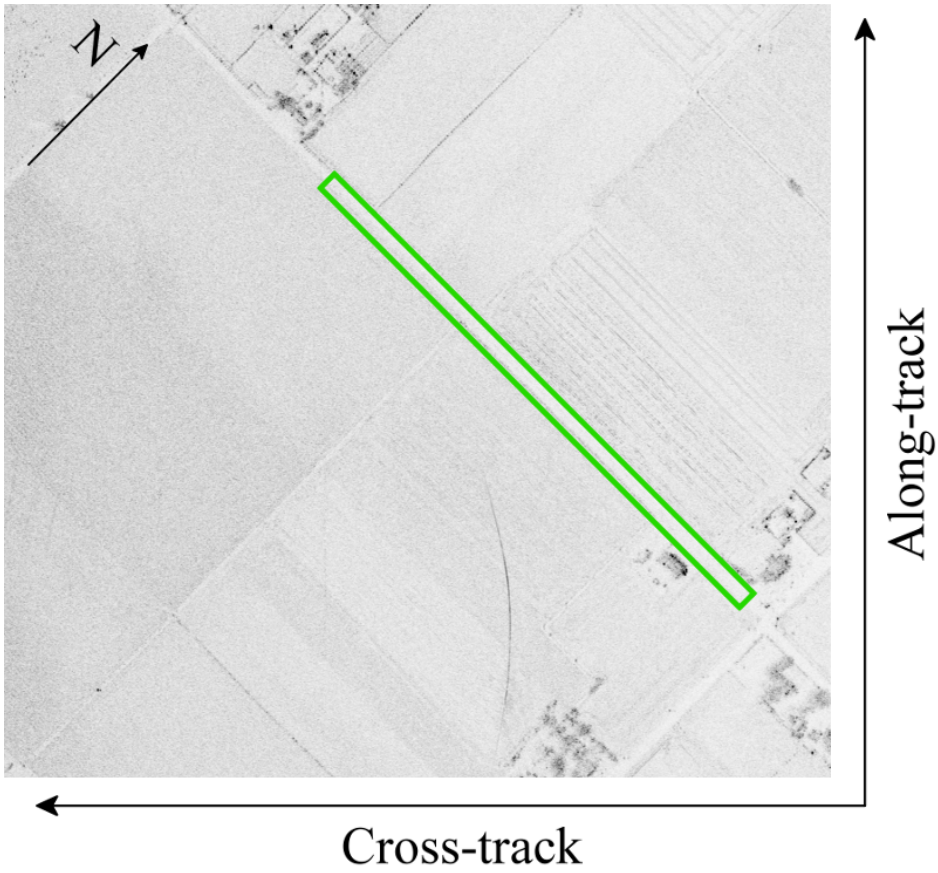

Figure 5.4: SAR image with bounding box highlighted for target's expected trajectory. By processing only the road traveled by the target, we reduce clutter, speed up processing, and enable finer pixel spacing with no loss of information during processing.

When operating on actual SAR data, we must deal with the problem of clutter, as discussed in Section 2.7. In general, clutter can be understood to refer to scatterers that interfere with the desired signal. In this thesis, clutter refers to any scatterer but the moving target. In my algorithm, I compute the AF by finding the peak pixel value of the image around the target. If that image includes large clutter values, it destroys my information about the moving target, so I restrict the size of image to exclude major sources of clutter. Because clutter generally has a high variance and since it can have a higher return than the moving target of interest, the AF formed from a section of the image that includes high clutter values is very noisy, as depicted in Fig. 5.5.

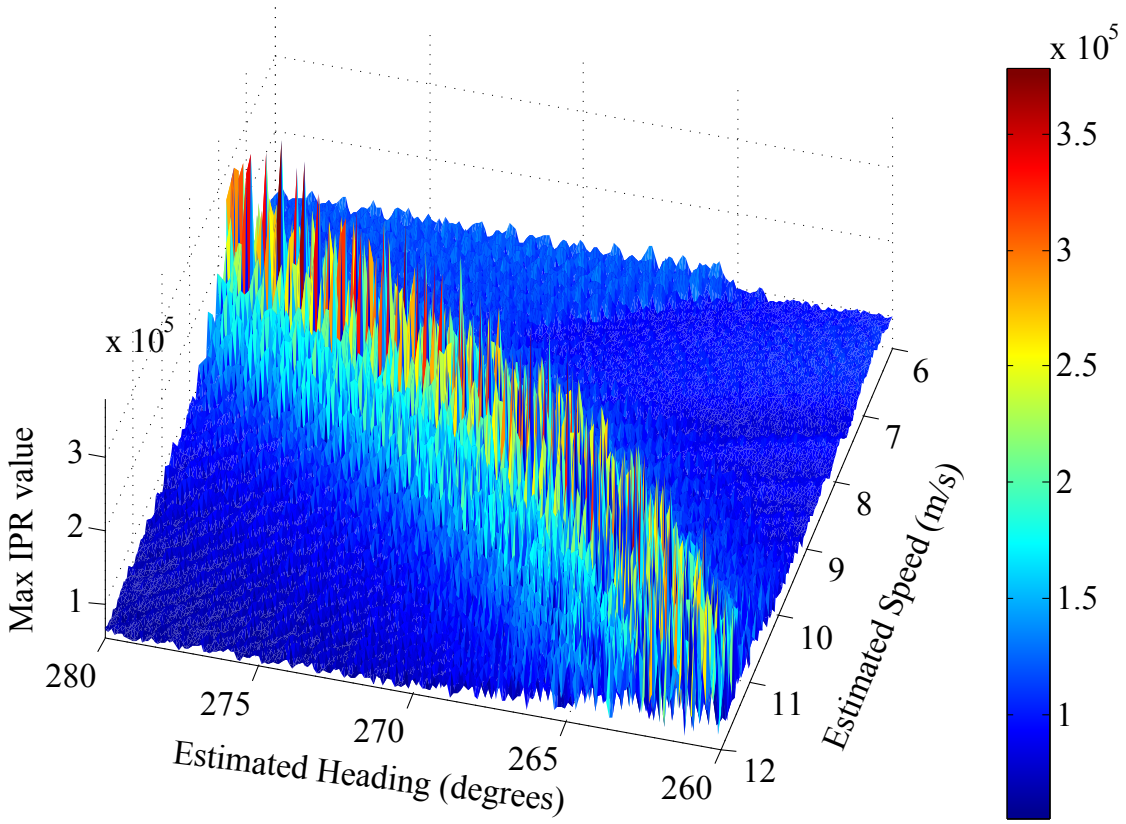

Figure 5.5: AF formed from a section of Fig. 5.2 that includes high clutter values. The occurrence of clutter in the SAR data my produce SAR returns with higher echo intensities than the moving target. In this case, the algorithm cannot find the target signal within the clutter. We alleviate this problem by constraining the bounding box to include just the road the moving target is on.

The clutter most prevalent in the data used in this thesis occurs mostly away from the roads. High clutter values are due to strong scatterers found in man-made structures like buildings and gates. In general, these scatterers are not immediately adjacent to roads, so a bounding box around a road mostly eliminates clutter caused by these scatterers. We can therefore assume that for the most part, in any image where a road bounding box is used, the highest peak value comes from the target's radar return.

Once we determine the appropriate bounding box, we choose a range of heading and speed values to use as motion compensation parameters in the backprojection algorithm. Consider one set of motion parameters ψ_1 and v_1 as an example. We pass the heading and speed into the backprojection algorithm, which operates on each pixel for each pulse in

the data collection. For each pixel during every pulse, the appropriate shift s is calculated according to the standard displacement equation

$$s(t) = s_0 + vt, \tag{5.2}$$

where s_0 is the initial displacement, v is velocity, and t is time. For our purposes, t is the number of pulses transmitted since the beginning of the collection which we call the "absolute pulse number," and v is the target velocity in m/pulse. t is calculated as the absolute pulse number minus the pulse number associated with the aircraft's point of closest approach to the target. This offset based on the point of closest approach is paramount to focusing the target in its true location. If it is not used, the target is away from its true position and in general is outside of the bounding box.

Since the image is formed from the vantage point of the radar, it is convenient to calculate the shift in terms of its cross- and along-track components. The cross- and along-track shifts s_x and s_y are given by

$$\begin{aligned} s_x(t) &= v_t t \sin(\psi_t) \\ s_y(t) &= v_t t \cos(\psi_t), \end{aligned} \tag{5.3}$$

where ψ_t is the target's heading and v_t is the target's speed. In Eq. (5.3), s_0 is set to zero because we are compensating only for motion, not for target position. Once we calculate the proper shift, we apply it to the current pixel and do this for every pixel for each pulse. This is done for every set of motion parameters we desire to include in the AF.

It is important to note that a moving target that is focused and whose motion is fully compensated with proper motion parameters is located in its true position, which we define as its position halfway through the radar collection. This is also known as the zero-Doppler line, as described in Section 3.2. Therefore, a target with any amount of along- and cross-track motion (assuming it is on the road during the SAR collection) appears on the road after motion compensation. It is for this reason that we can confidently constrain the SAR imaging box to the road the target is traveling on. Likewise, applying incorrect motion

parameters to a SAR image of a moving target may shift the target far outside the bounding box so it is not even visible in the final image.

Once the set of individual motion-compensated SAR images are formed for the corresponding range and precision of motion parameters, we iterate through this set of images in MATLAB to find the peak pixel value of each image. As discussed in the previous paragraph, it is safe to assume that with the correct motion parameters, the target appears on the road. We also assume that barring any dominant scatterers in the image when the target is not present, the radar returns in the image are generally low. Therefore, the peak value in the image almost certainly comes from the target when it is present.

Once the maximum value in each image is found, we generate a 3-D plot of the values on a 2-D grid corresponding to the range and precision of motion estimates used in AF processing. This 3-D plot is the AF. The AF for the SAR data depicted in Fig. 5.2 is shown in Fig. 5.6.

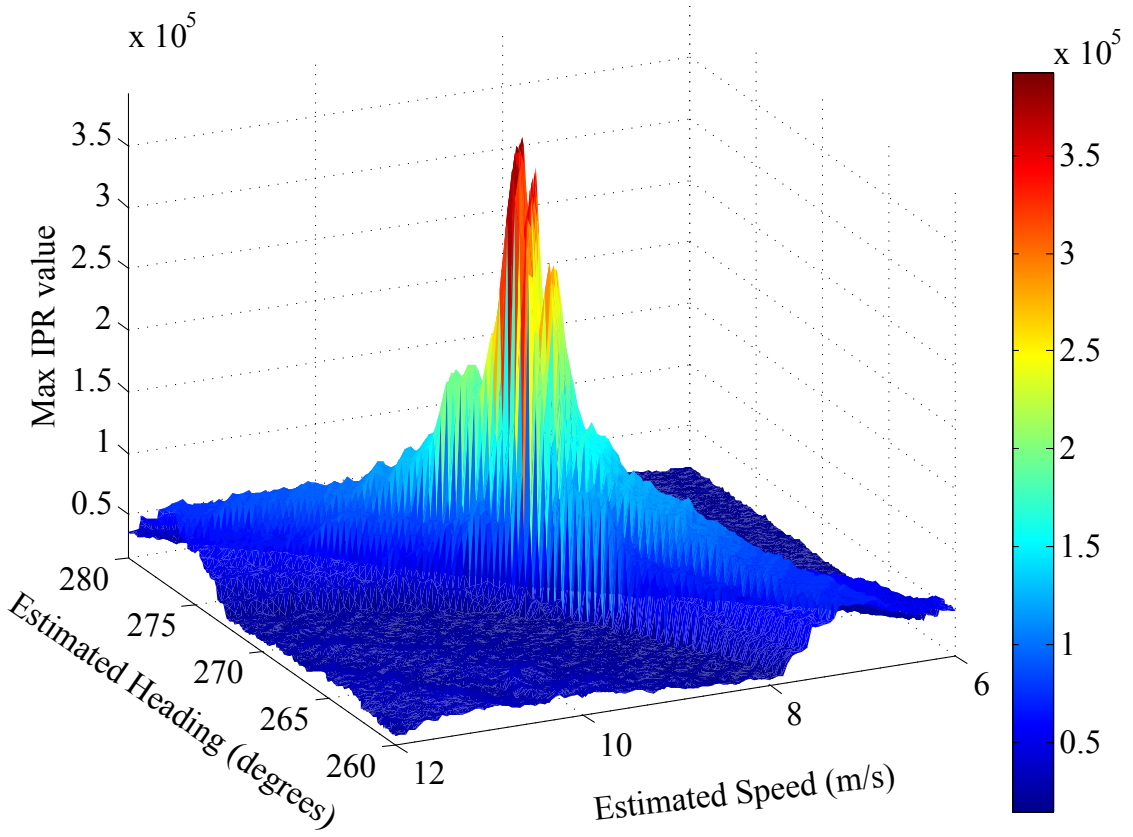

Figure 5.6: AF for moving target depicted in Fig. 5.2. The peaks correspond with high peak values in the motion-compensated SAR images as a result of sharp image focus.

As described in Chapter 4, the last step of the algorithm is to find the target speed associated with the known target heading. If necessary, we process the AF again for a smaller range of motion parameters but with finer precision. Figure 5.7 shows lines drawn from the AF peak to each axis in order to show the combination of motion parameters that are closest to the actual motion of the target during the SAR collection. Since this is actual data and the vehicle does not have perfectly uniform motion, the peak in the AF may vary slightly from the known road heading.

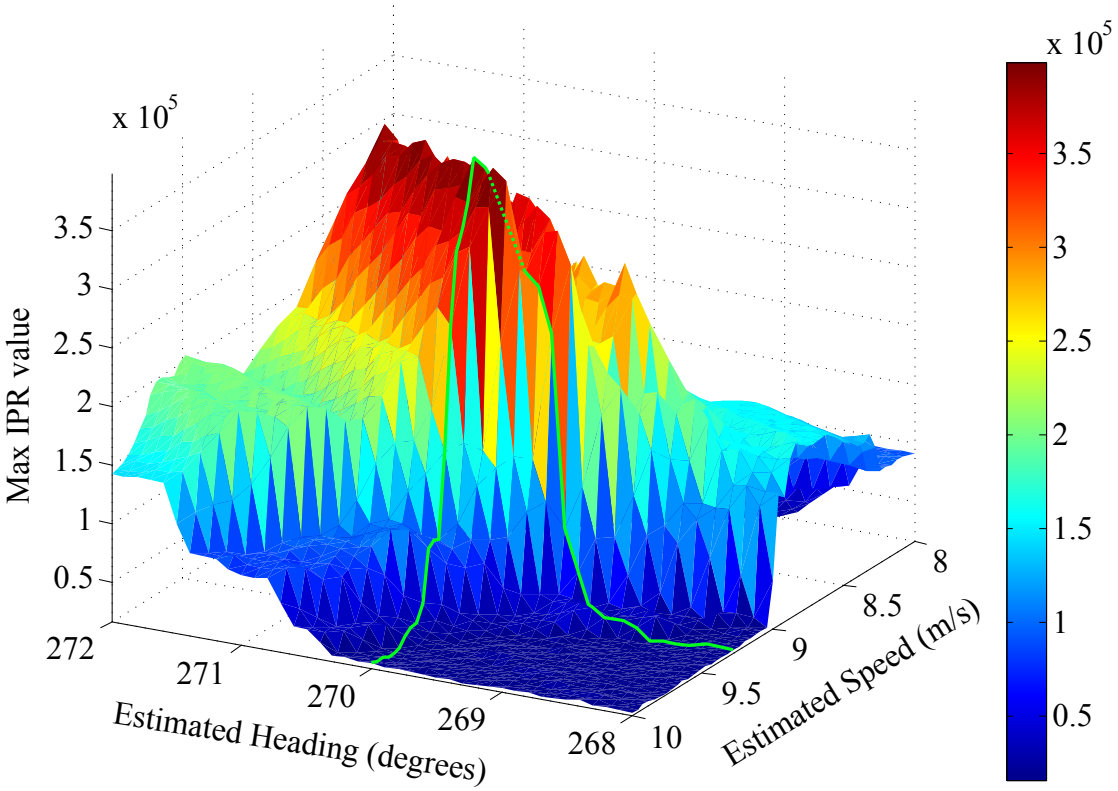

Figure 5.7: AF for moving target depicted in Fig. 5.2. Lines have been drawn from the AF peak to each motion parameter axis to show the most likely motion parameters of the target. The AF peak associated with the road heading is at 270°, 9.28 m/s.

5.1.4 Application of Motion Parameter Estimates to SAR Data

Once we know the correct target motion parameters, applying them to SAR data results in a reasonably well-focused image of the target, as shown in Fig. 5.8. For convenience, the focused image of the moving target is superimposed on the original stationary SAR image and is shown in Fig. 5.9.

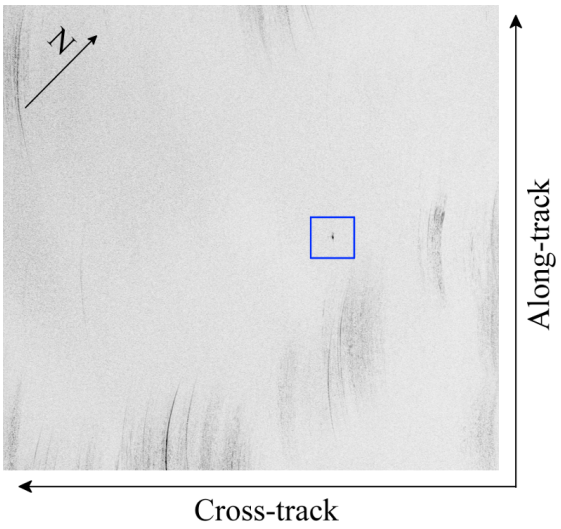

Figure 5.8: SAR data depicted in Fig. 5.2 processed with motion compensation parameters of 270° and 9.28 m/s. While the target is focused, note that the stationary clutter is now smeared because of the applied motion compensation.

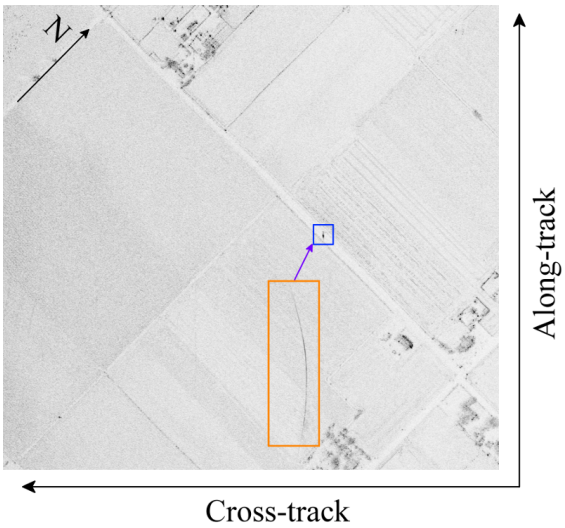

Figure 5.9: SAR data depicted in Fig. 5.2 superimposed with focused image of target processed with motion parameters of 270° and 9.28 m/s. The target is relatively well-focused and is located on the road at the radar's point of closest approach, as we expect for matching motion parameters.

5.2 Case Studies

This section provides a brief analysis of the algorithm's performance for various types of target motion, including strictly along-track motion, strictly cross-track motion, and a combination of both. Each subsection examines one of these three types of motion in actual SAR data and for specific target motion briefly discusses: (1) the stationary SAR image and reported truth data for the target's motion parameters; (2) the ambiguity function associated with the SAR data; (3) the motion-compensated image formed by applying the motion parameter estimates in backprojection processing.

5.2.1 Along-Track Target Motion

In SAR data with targets that exhibit along-track motion, the stationary SAR image of those targets is smeared. In this subsection we consider only targets that move strictly in the along-track direction. Figure 5.10 shows a stationary SAR image of an along-track moving target moving at 179.2°, 2.2 m/s. The image of the target is smeared but located on the road because there is no cross-track component of motion. Figure 5.11 and Fig. 5.12 are the corresponding AFs for that data and have wide and narrow motion parameter grids, respectively. Finally, Fig. 5.13 shows the focused target that has been processed with the estimated motion parameters (177.8°, 1 m/s) superimposed on the original stationary SAR image.

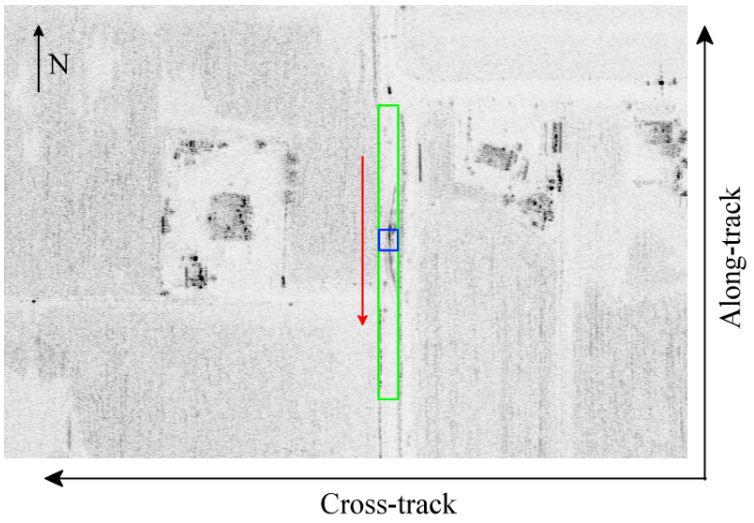

Figure 5.10: SAR image with target moving at 179.2°, 2.2 m/s on the road as indicated by the red arrow, which has been moved off of the road for visibility of the target but still gives the target's path during the collection. Since the target smear is contained to the road, we know it has strictly along-track motion, and since the target smear is concave in towards the flight track, we know it moves in the opposite direction as the radar. The blue box represents the target's true position at halfway through the SAR collection. The bounding box is highlighted in green and represents the area processed for the AF.

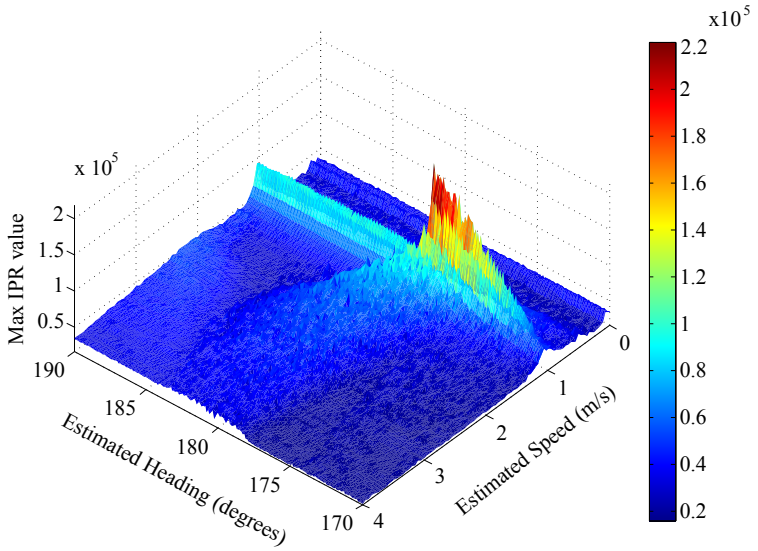

Figure 5.11: Ambiguity function for the SAR data in Fig. 5.10 with wide range of heading and speed values. This AF is formed processing the SAR data only for the green bounding box in Fig. 5.10. Note the ambiguity curve that lies along the 1 m/s mark.

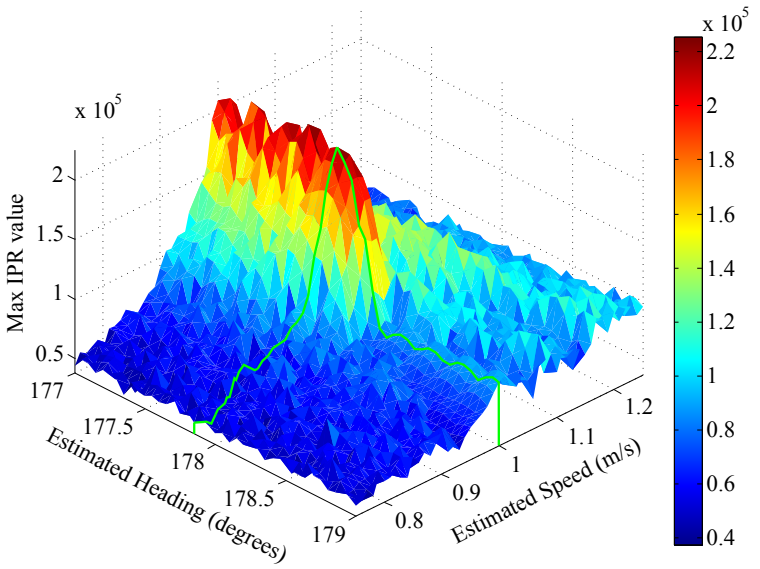

Figure 5.12: Ambiguity function processed with smaller range of values but finer precision than Fig. 5.11. A line has been drawn to the peak nearest the road's heading of 179.2°. This peak lies at 177.8°, 1 m/s. These motion parameters are this algorithm's best estimate of the true target motion.

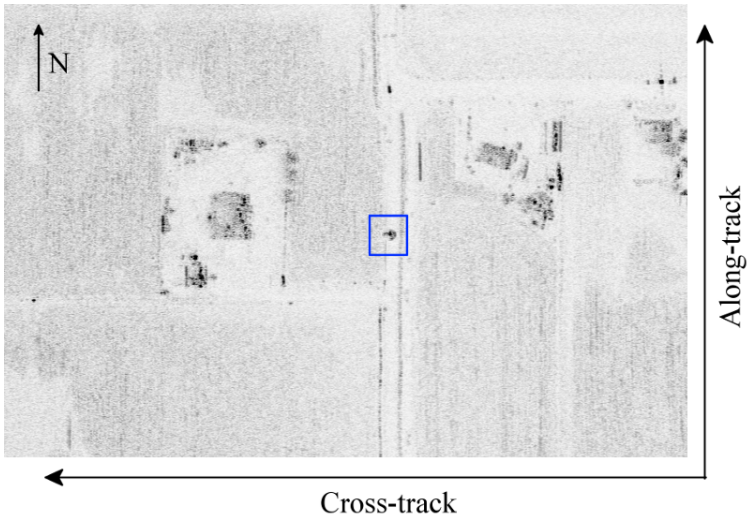

Figure 5.13: Focused target image superimposed on SAR image from Fig. 5.10. The motion parameters derived from the AF and applied to this target are 177.8°, 1 m/s. The target has been highlighted in blue for visibility on top of the original target smear.

Figures 5.14 to 5.17 show the stationary SAR image, ambiguity functions, and focused target image for an along-track moving target from a different data collection. In this case, the target moves at 0°, 6.7 m/s. The AF-derived best estimate of the target's motion is -0.5°, 3.11 m/s.

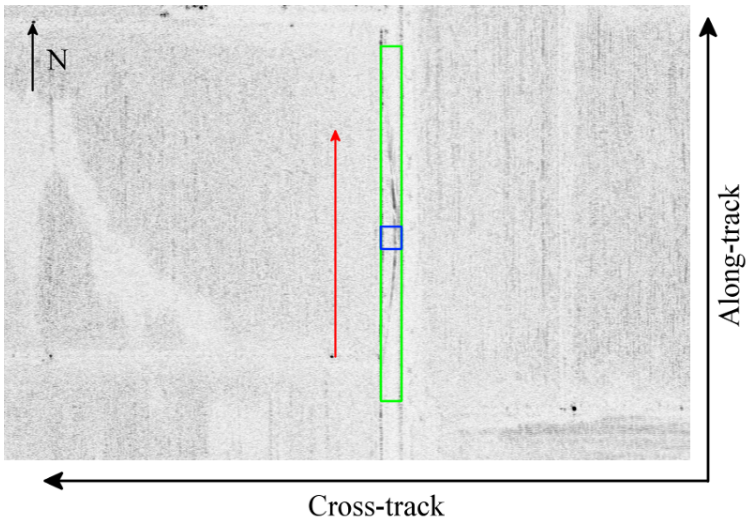

Figure 5.14: SAR image of target moving at 0°, 6.7 m/s on the road as indicated by the red arrow, which has been moved off of the road for visibility of the target but still gives the target's path during the collection. Since the target smear is contained to the road, we know it has strictly along-track motion, and since the target smear is concave out from the flight track, we know it moves in the same direction as the radar. The blue box represents the target's true position at halfway through the SAR collection. The bounding box is highlighted in green and represents the area processed for the AF.

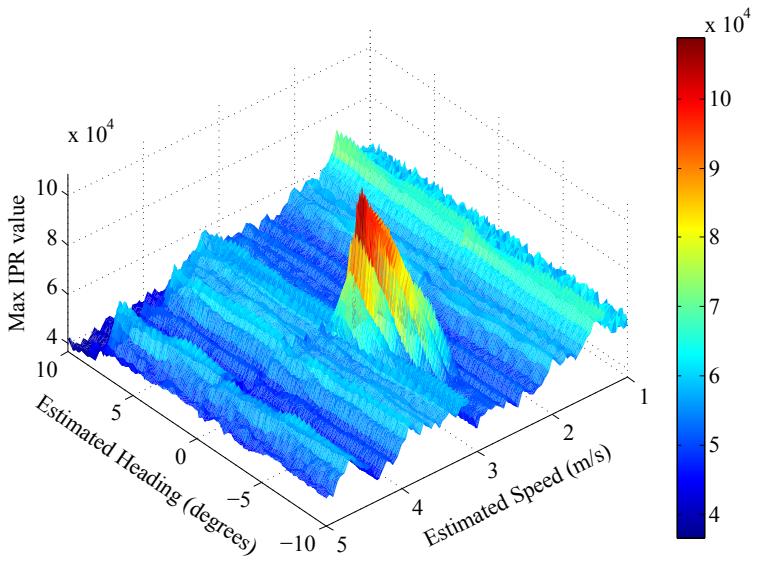

Figure 5.15: Ambiguity function for the SAR data in Fig. 5.14 with wide range of heading and speed values. This AF is formed processing the SAR data only for the green bounding box in Fig. 5.14. Note the ambiguity curve that lies along the 3.1 m/s mark.

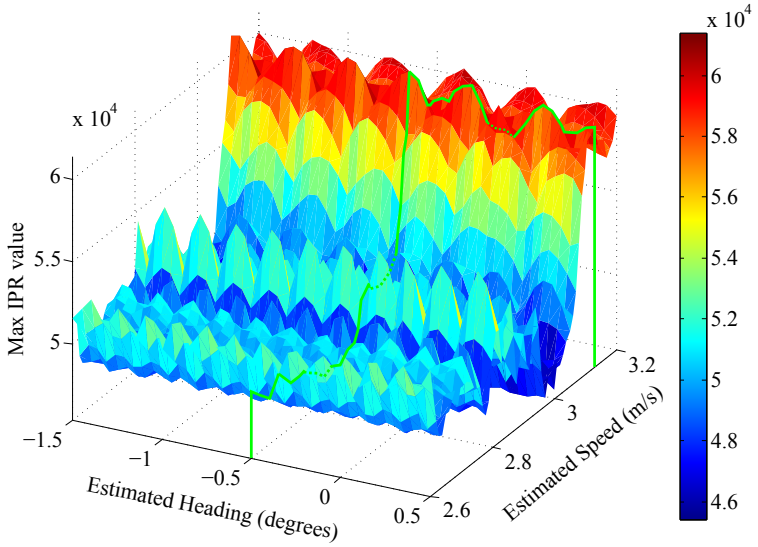

Figure 5.16: Ambiguity function processed with smaller range of values but finer precision than Fig. 5.15. A line has been drawn to the peak nearest the road's heading of 0°. This peak lies at -0.5°, 3.11 m/s. These motion parameters are this algorithm's best estimate of the true target motion.

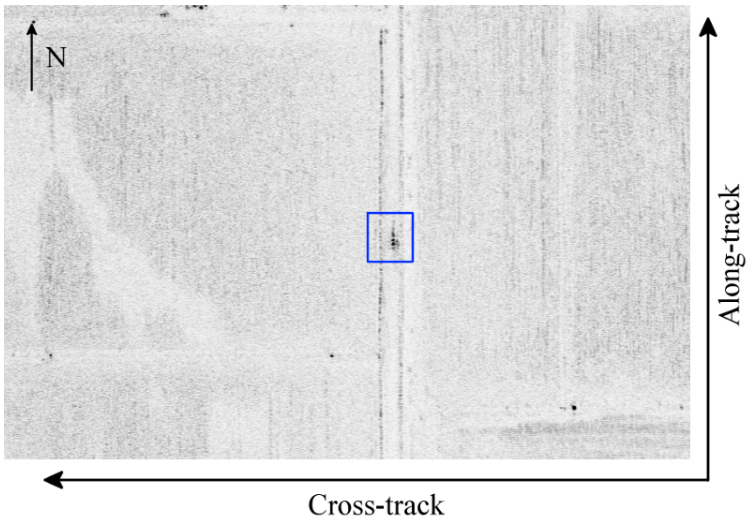

Figure 5.17: Focused target image superimposed on SAR image from Fig. 5.14. The motion parameters derived from the AF and applied to this target are -0.5°, 3.11 m/s. The target has been highlighted in blue for visibility on top of the original target smear.

5.2.2 Cross-Track Target Motion

As opposed to along-track motion, strictly cross-track motion induces no image smearing in SAR. Instead of smearing, targets with cross-track motion shift in azimuth from their true positions. Figure 5.18 shows a stationary SAR image of a cross-track moving target that is well focused but not in its correct location. Figure 5.19 and Fig. 5.20 depict the ambiguity functions associated with this data. In Fig. 5.21, the focused target image is superimposed on the stationary SAR image. The true motion parameters for this target are 90.15°, 2.2 m/s and the best estimate is 90.5°, 1.1 m/s.

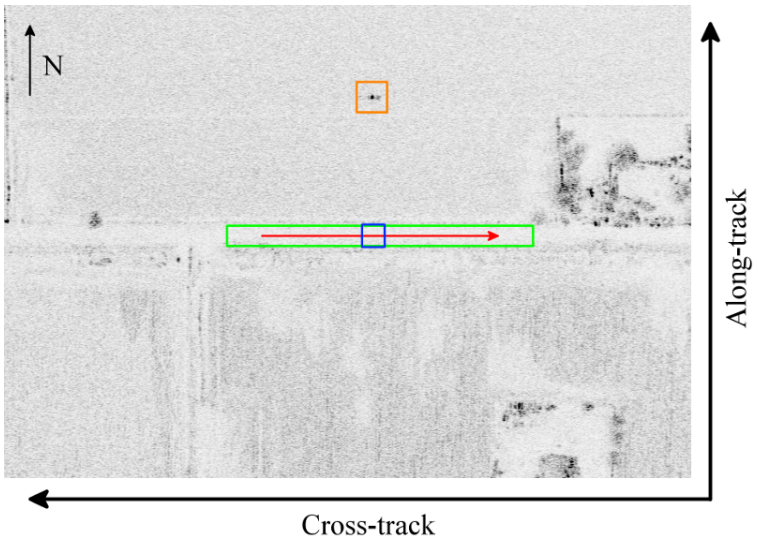

Figure 5.18: SAR image with target moving at 90.15°, 2.2 m/s on the road as indicated by the red arrow, which shows the target's path during the collection. Since the target is well focused but shifted from the road, we know that the motion is strictly cross track. The blue box represents the target's true position at halfway through the SAR collection. The bounding box is highlighted in green and represents the area processed for the AF.

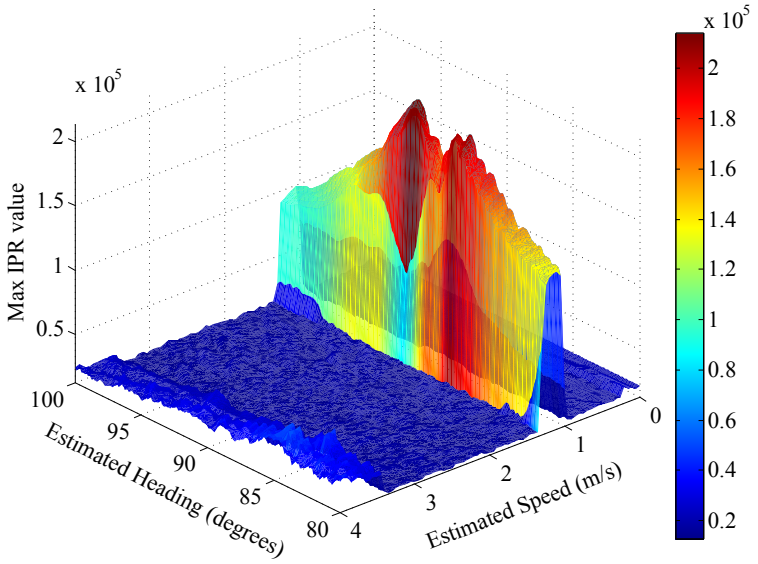

Figure 5.19: Ambiguity function for Fig. 5.18 with wide range of heading and speed values. This AF is formed processing the SAR data only for the green bounding box in Fig. 5.18. Notice the ambiguity curve that lies along the 1.1 m/s mark.

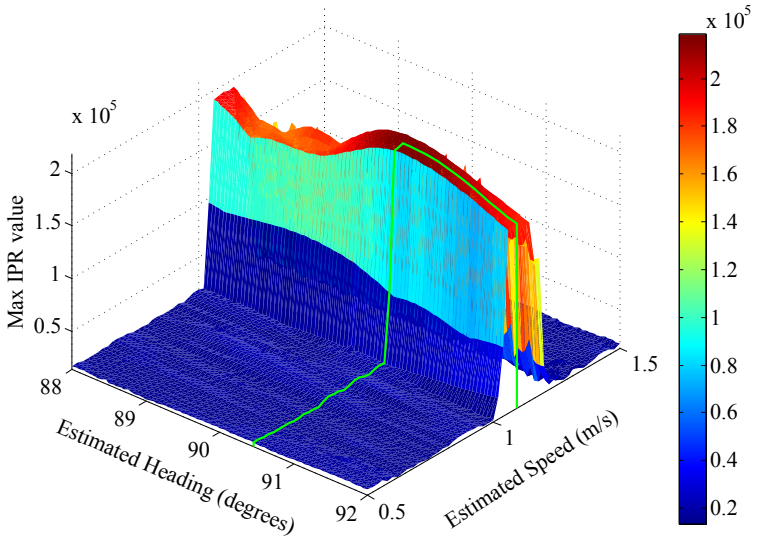

Figure 5.20: Ambiguity function processed with smaller range of values but finer precision than Fig. 5.19. A line has been drawn to the peak nearest the road's heading of 90.15°. This peak lies at 90.5°, 1.1 m/s. These motion parameters are this algorithm's best estimate of the true target motion.

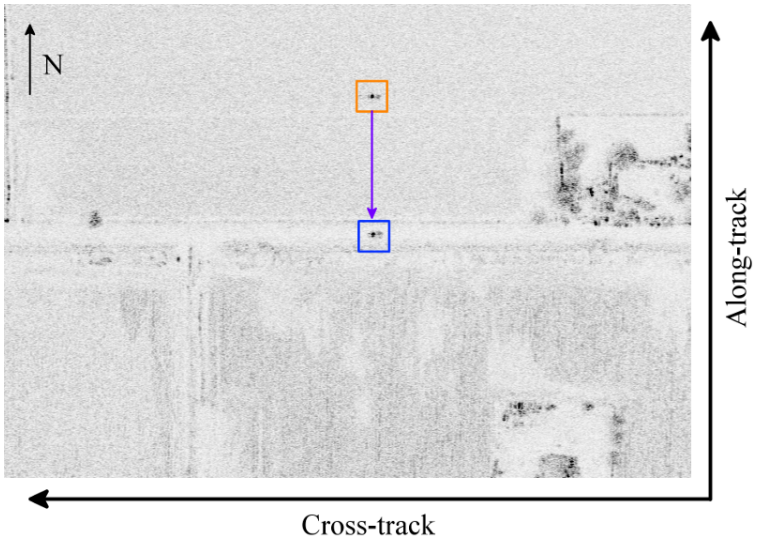

Figure 5.21: Focused target image superimposed on stationary SAR image from Fig. 5.18. The motion parameters derived from the AF and applied to this target are 90.5°, 1.1 m/s. The target has been highlighted in blue for visibility in its true position at halfway through the data collection.

5.2.3 Combined Target Motion

Target motion with along- and cross-track components of motion induces both smear and shift to the target image. This subsection outlines a case with a combined-motion target moving at 89.6°, 2.2 m/s. As with the previous subsections in Section 5.2, here I show the stationary SAR image, ambiguity functions, and focused target image for a target motion estimate of 90.15°, 1.1 m/s.

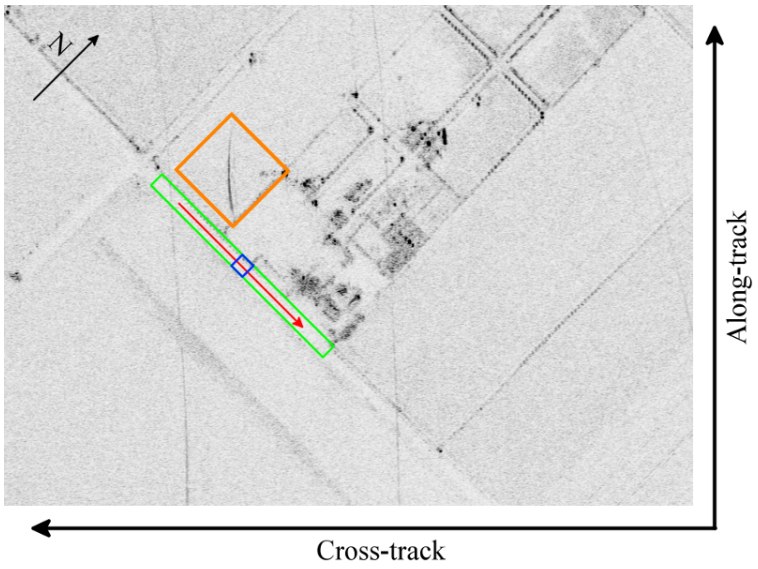

Figure 5.22: SAR image with target moving at 89.6°, 2.2 m/s on the road as indicated by the red arrow, which shows the target's path during the collection. Since the target image is smeared and shifted from the road, we know it has both along- and cross-track motion. The blue box represents the target's true position at halfway through the SAR collection. The bounding box is highlighted in green and represents the area processed for the AF.

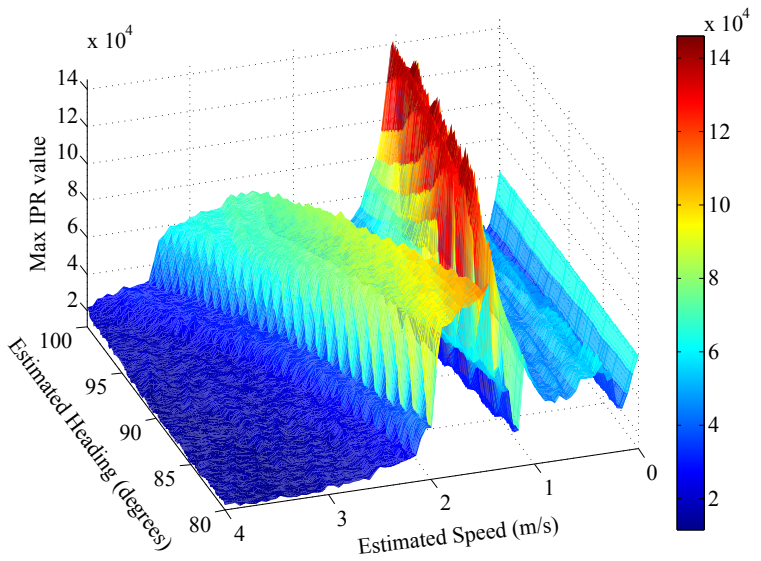

Figure 5.23: Ambiguity function for Fig. 5.22 with wide range of heading and speed values. This AF is formed processing the SAR data only for the green bounding box in Fig. 5.22. Notice the ambiguity curve that lies along the 1.1 m/s mark.

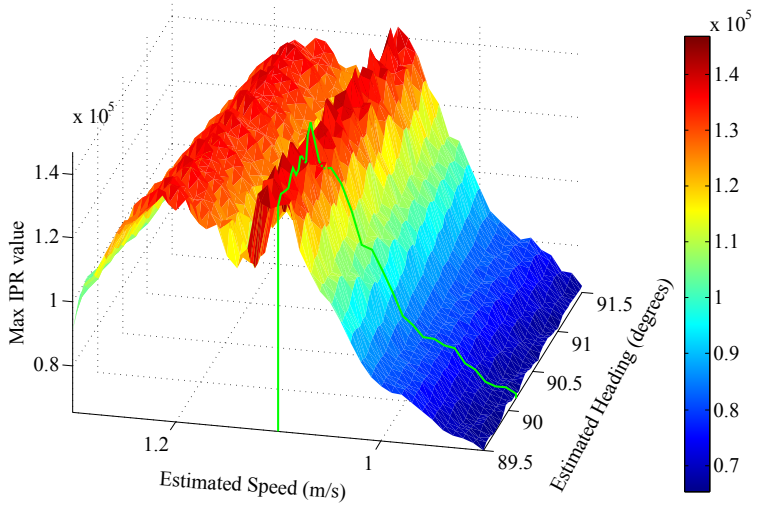

Figure 5.24: Ambiguity function processed with smaller range of values but finer precision than Fig. 5.23. A line has been drawn to the peak nearest the road's heading of 89.6°. This peak lies at 90.15°, 1.1 m/s. These motion parameters are this algorithm's best estimate of the true target motion.

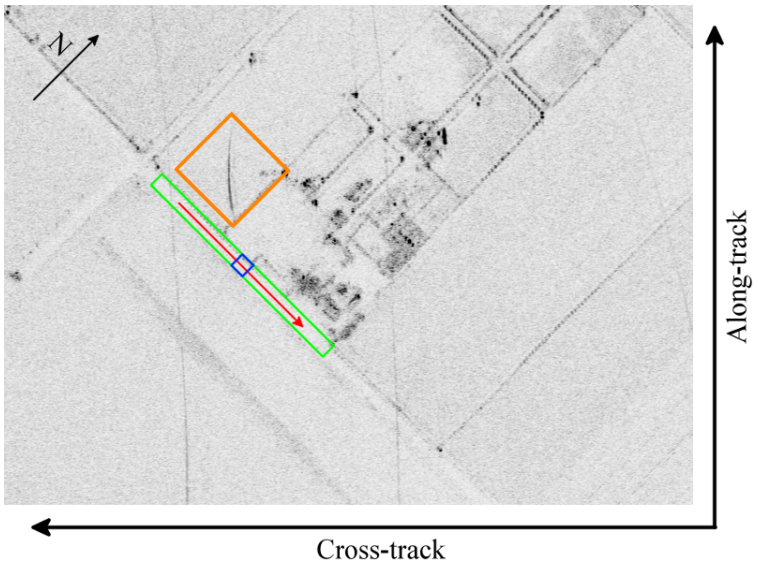

Figure 5.25: Focused target image superimposed on SAR image from Fig. 5.22. The motion parameters derived from the AF and applied to this target are 90.15°, 1.1 m/s. The target has been highlighted in blue for visibility on top of the original target smear.

5.3 Error Analysis

Since the SAR data used in this chapter has accompanying truth data, we can perform an analysis of the algorithm's performance by comparing its motion estimates to the truth information. A table of error results for the tests performed on actual SAR data is given in Table 5.1. The errors in the results come from several sources. A key issue is the quality of the "truth" data, which was gathered as follows. A two-way radio link was made between the radar and vehicle operators. As the aircraft flew by to start each data collection, the radar operator requested that the driver maintain a particular target speed throughout the collection. The driver attempted to maintain a constant speed as close to the target speed as possible with the speedometer as the only indication to his speed; there was no independently-recorded vehicle speed. The reported truth data is the vehicle speed requested by the radar operator. Therefore, while the target speed may be reported as constant, the actual speed may be different than the recorded speed by a constant with some variability because of operator error. Unfortunately, GPS data for the target is unavailable, so there is no way of confirming the true motion of the target.

Table 5.1: Error results for five cases of moving target parameter estimation in actual SAR data.

Heading			Speed		
Truth (°)	Estimate (°)	Error (°)	Truth (m/s)	Estimate (m/s)	Error (%)
269.7	270	0.3	11.1	9.28	16.4
179.2	177.8	1.4	2.2	1	55
0	-0.5	0.5	6.7	3.11	54
90.15	90.5	0.35	2.2	1.1	50
89.6	90.15	0.55	2.2	1.1	50

A discussion of the algorithm's performance results is warranted. Because the vehicle is constrained to the road, we do not expect much variance in the error of the target heading estimate. This is confirmed in Table 5.1 with consistently low error in target heading estimates. On the other hand, target speed estimate error is typically high. However, upon closer analysis of the motion-compensated SAR images, we find that the images often do not focus at the reported truth speed which we believe may be incorrect.

We desire to demonstrate the accuracy of the AF-derived target motion estimates. In the following analysis, we examine the SAR images of two different targets processed with various speeds for motion compensation. The heading used in motion compensation is assumed to be the heading found in the AF for each of these targets. We examine just the targets within the SAR images to determine where they are located and how they focus. In the case of along-track motion, the target is focused to a small point when its motion is properly compensated. In the case of strictly cross-track target motion, the target's true position is the middle of the road it is traveling on and will focus to that point with proper motion compensation.

Consider the stationary SAR image in Fig. 5.10 as an example of strictly along-track target motion. The reported target speed is 2.2 m/s and as expected, the along-track image smear is concave in towards the aircraft, corresponding to the reported 179.2° target heading. Figure 5.26 shows a progression of speed compensation at a constant heading of 177.8°, which is the AF-derived target heading estimate in Fig. 5.12. When we use the reported true speed for motion compensation, the target is actually focused worse than the stationary SAR image. We observe that the compensated speed is too much after 1.0 m/s

because the target begins to smear again and the concavity of the target smear changes. This result confirms the AF-estimated speed of 1.0 m/s even though the reported true speed is 2.2 m/s.

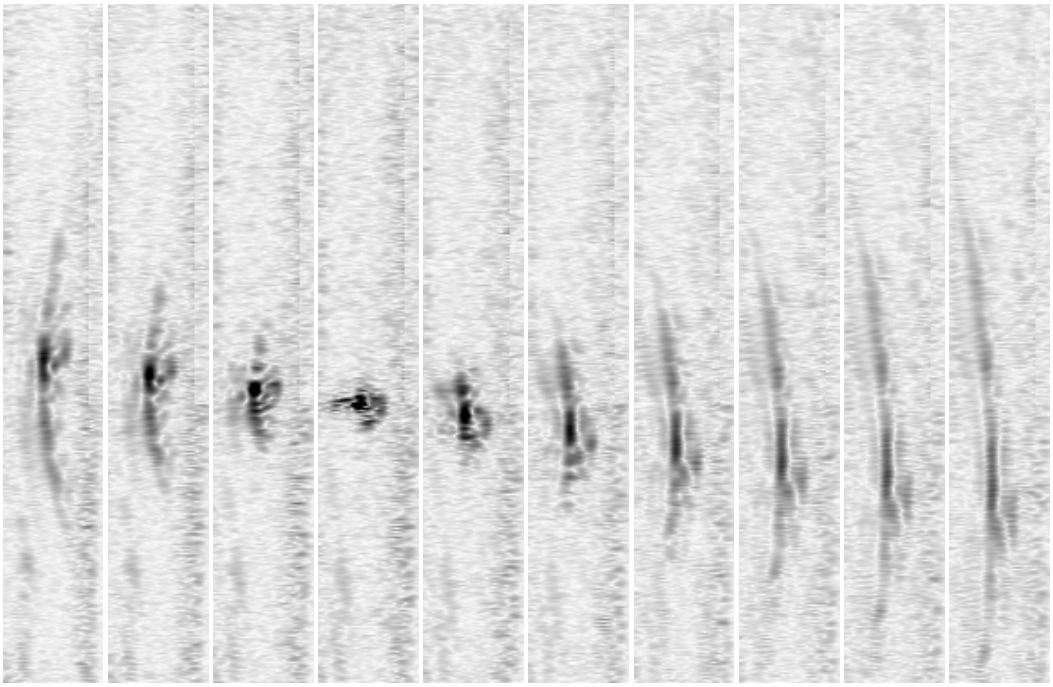

0.4 0.6 0.8 1.0 1.2 1.4 1.6 1.8 2.0 2.2 (m/s)

Figure 5.26: Sequence of images of along-track moving target for varying speed compensation. Reported target motion is 179.2°, 2.2 m/s. Incorrect motion compensation produces an unfocused image that is stretched out in the along-track direction and curved, whereas the most correct motion compensation produces an image that is localized to a small area. Each image contains only the road traveled by the target and is as wide as that road. All images are processed at 177.8° at varying speeds which increase from left to right. Moving from left to right, note that the image starts smeared, focuses at 1.0 m/s, and defocuses from that point.

Now let us consider strictly cross-track motion, as found in the stationary SAR image of Fig. 5.18. Since the target is moving towards the aircraft with strictly cross-track motion, we expect the target to be well focused but shifted above the road. Since the target is traveling on the middle of the road, we expect that with correct motion compensation, it will be focused to that position. At the AF-derived motion estimates of 90.5°, 1.1 m/s, the image focuses well and is located at its true position in the middle of the road, as shown

in Fig. 5.21. Figure 5.27 shows a series of motion-compensated SAR images with varying compensated speed. Since each image contains only the road traveled by the target, when the wrong speed is used for motion compensation, the target shifts out of the image. As we sweep the applied speed compensation from 1.04 m/s to 1.18 m/s, the target shifts onto the road from above and off the road in the opposite direction, as shown in Fig. 5.27. This change in shift is the cross-track equivalent of the along-track target smear changing concavity in the previous example. When compensating for the target's motion at the reported speed of 2.2 m/s, the target is far outside of the bounding box, not on the road at its true position. When using the AF-estimated motion parameters for motion compensation, the target focuses to its proper position on the road. This behavior confirms the accuracy of the 1.1 m/s estimate even though the reported target speed is 2.2 m/s. Furthermore, the fact that the AF-derived speed estimates in Table 5.1 produce focused targets but are up to 50% less than the reported truth speed indicates a mean error in reported versus actual vehicle speed.

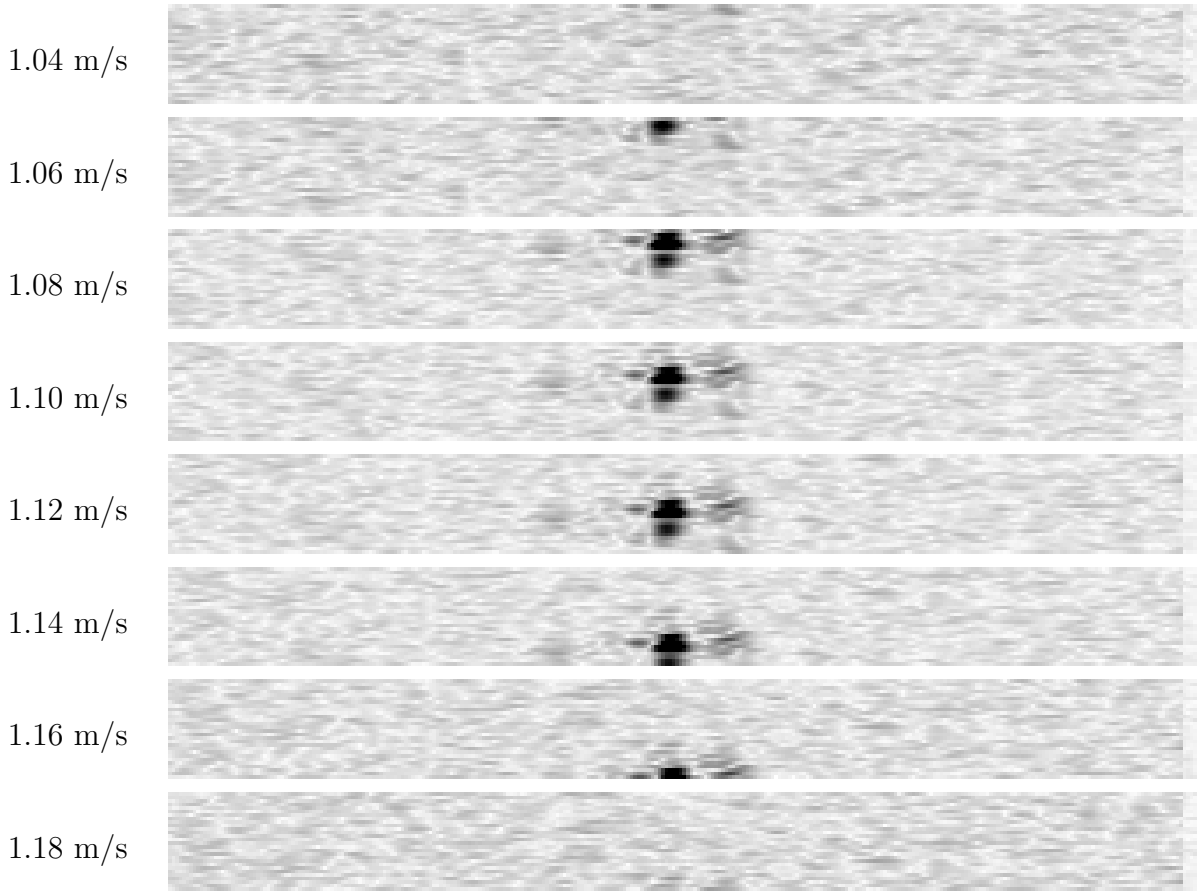

Figure 5.27: Images of target moving on cross-track road with varying speed compensation. Each image contains only the road traveled by the target. Since the target is moving to the right in each image, when its motion is properly compensated, the target appears in the middle of the road, which is the vertical center of each image. The reported target motion is 90.15°, 2.2 m/s. All images are processed at 90.5° at varying speeds which increase from top to bottom. Moving from top to bottom, note that the target starts outside of the image, focuses to the middle of the road at 1.1 m/s, and leaves the image at 1.18 m/s.

In all cases, my algorithm estimates a slower target speed than the reported truth data. For strictly along-track motion, no better image focus is had than using the motion estimates derived from the AF. When the reported true target speed is used for motion compensation, the target is generally smeared because the speed is too high. In strictly cross-track motion, the target is focused *on the road* in its correct location when using the motion parameters found from the AF. However, when the reported truth speed is used for motion compensation, the target shifts off the road and out of the bounding box in the direction opposite the initial shift in the stationary SAR image. For combined along- and

cross-track motion, both smearing and shifting are present when using reported truth data for motion compensation, and the best target location and focus results from using the estimated motion parameters. These results suggest that the reported truth data overestimates the actual target speeds.

The results in this chapter show that this algorithm is practical for use with actual SAR data. The AF formed from real data works as expected based on the results for simulated data. Several types of uniform motion are studied, including strictly cross- and along-track motion and a combination of both at various target speeds. Applying the AF-derived motion estimates as motion compensation parameters to the original SAR data produces well-focused images of moving targets in their correct locations. Although errors in the estimated target speeds tend to be high based on comparison to reported vehicle speeds, these errors may be a result of inaccurate reporting of the target speeds.

Chapter 6

Conclusion

Moving targets are smeared and/or shifted in SAR images. Target motion can be extracted using interferometry, but that requires the use of two antennas. It is shown in previous work that the GMTI solution for a moving target in single-channel SAR is underdetermined. However, by constraining the target's motion to a straight road, we eliminate one variable in the GMTI solution and it becomes solvable. This thesis presents a practical, although computationally expensive algorithm, for estimating target motion in single-channel SAR data.

The algorithm performs backprojection processing on a single SAR data collection with a suspected moving target. Backprojection is performed for a variety of motion estimates, during which, for each set of motion parameters, the entire image grid is shifted with the motion parameter. The result of this process is a large set of images with different levels of focus and target motion compensation. Ideally, at least some images have good target image focus. In general, since image focus improves when the target return is higher and narrower, an image of a moving target has its highest radar return when it is fully focused with proper motion parameters. By examining the target peak of each image in this large set of processed images, we can determine which set of motion parameters best estimates the true target motion. These peaks are evident in the AF, which is essentially a matched filter for the moving target.

Without some constraint on our data, however, there are many combinations of motion that produce target images that look identically well-focused. This is seen in the AF, where there is usually a dominant ambiguity curve that represents the motion parameters the produce identical target image focus. I analyze a sample set of simulated SAR data processed with the motion parameters corresponding to this ambiguity curve. Visually, it

is difficult to distinguish the image resulting from one set of motion parameters from that of another set. The use of a contrast ratio metric confirms that even on a quantitative basis, the target images processed with the motion parameters lying on the ambiguity curve have very similar image focus. This analysis shows that image focus alone is insufficient for determining target motion parameters in SAR. The basis of my algorithm is constraining the target to have uniform velocity on a straight road during the SAR collection. I then process the AF for a range of motion parameters around the constraint. By choosing the peak in the AF corresponding to the constrained road heading, I effectively limit the target motion estimates to a single heading and speed. By processing the original SAR data with this single motion estimate, the result is generally a well-focused image of the target.

In this thesis, I apply this algorithm to both simulated and actual SAR data. It works well in both cases, although there are some differences between the estimates for actual data and ground truth. Some of this error is caused by non-linear aircraft and target motion and is unavoidable. To minimize error and processing time, I choose a bounding box around the straight road on which the target travels so I only process relevant data. This speeds up processing and significantly reduces image clutter, thus enabling more accurate motion estimates. I demonstrate my algorithm's facility with tests on targets with varying speeds having along-track motion, cross-track motion, and a combination of both. I show that based on target image focus and location, the algorithm chooses accurate motion parameters.

6.1 Future Work

This work is only initial and was done with favorable conditions. The algorithm in this thesis can be improved by exploring more conditions of motion and clutter. Some future work includes:

- Extend this work to complicated ground motion including curved paths and non-linear acceleration.
- The asphalt roads this thesis' actual SAR data have low clutter. Examine the effect on the algorithm when targets are traveling on dirt or cement, or when other moving vehicles are present on the road.

- Improve the algorithm's robustness to handle clutter in a larger imaging grid with a better target return discrimination technique.
- Investigate time-frequency analysis for SAR GMTI using backprojection.
- Investigate the feasibility of using techniques for single-channel SAR target motion estimation with backprojection that have previously only been used with frequency-domain algorithms, such as Keystone transforms.
- Extend the algorithm to work for 3-D motion exhibited by maritime targets.

Bibliography

[1] M. I. Skolnik, *Introduction to Radar Systems*, 3rd ed. New York, NY: McGraw-Hill, 2001. 1, 28

[2] J. Winkler, ""An Investigation of Ground Moving Target Indication (GMTI) with a Single-Channel SAR System"," Master's thesis, Brigham Young University, 2013. 2, 17, 21, 22, 23, 25, 26, 27, 28, 29, 30, 31, 39

[3] M. A. Richards, J. A. Scheer, and W. A. Holm, *Principles of Modern Radar*. Edison, NJ: SciTech, 2010. 5, 6, 7, 10, 12, 18, 19, 22, 27, 30, 32, 44

[4] E. Zaugg, ""Generalized Image Formation for Pulsed and LFM-CW Synthetic Aperture Radar"," Ph.D. dissertation, Brigham Young University, 2010. 9, 15, 41

[5] F. T. Ulaby, D. G. Long, A. K. Fung, and R. K. Moore, *Microwave Remote Sensing Modern Edition*. Norwood, MA: Artech House, 2013. 10, 11, 19

[6] P. Loughlin and L. Cohen, "The uncertainty principle: global, local, or both?" *Signal Processing, IEEE Transactions on*, vol. 52, no. 5, pp. 1218–1227, May 2004. 10

[7] "Radiation pattern," http://en.wikipedia.org/wiki/Radiation_pattern, February 2014, accessed: 20 Mar 2014. 13

[8] W. L. Stutzman and G. A. Thiele, *Antenna Theory and Design*, 3rd ed. Hoboken, NJ: Wiley, 1998. 12

[9] F. Jay, Ed., *IEEE Standard Dictionary of Electrical and Electronic Terms*, 3rd ed., ser. ANSI/IEEE Std 100-1984. New York, NY: IEEE Press, 1984. 14, 15

[10] E. F. Knott, M. T. Tuley, and J. F. Shaeffer, *Radar Cross Section*, 2nd ed. Norwood, MA: Artech House, 2004. 14

[11] I. Cumming, Y. Neo, and F. Wong, "Interpretations of the omega-k algorithm and comparisons with other algorithms," in *Geoscience and Remote Sensing Symposium, 2003. IGARSS '03. Proceedings. 2003 IEEE International*, vol. 3, July 2003, pp. 1455–1458. 15

[12] I. G. Cumming and F. H. Wong, *Digital Processing of Synthetic Aperture Radar Data: Algorithms and Implementation*. Norwood, MA: Artech House, 2005. 16, 18

[13] "Shutter speed," http://en.wikipedia.org/wiki/Shutter_speed, March 2014, accessed: 16 Apr 2014. 22

[14] J. K. Jao, "Theory of synthetic aperture radar imaging of a moving target," *Geoscience and Remote Sensing, IEEE Transactions on*, vol. 39, no. 9, pp. 1984–1992, Sep 2001. 22, 23, 24

[15] M. Kirscht, "Detection and imaging of arbitrarily moving targets with single-channel sar," in *RADAR 2002*, Oct 2002, pp. 280–285. 22

[16] R. Raney, "Synthetic aperture imaging radar and moving targets," *Aerospace and Electronic Systems, IEEE Transactions on*, vol. AES-7, no. 3, pp. 499–505, May 1971. 22, 24, 25

[17] S. Barbarossa, "Detection and imaging of moving objects with synthetic aperture radar. 1. optimal detection and parameter estimation theory," *Radar and Signal Processing, IEE Proceedings F*, vol. 139, no. 1, pp. 79–88, Feb 1992. 22

[18] V. C. Chen and H. Ling, *Time-Frequency Transforms for Radar Imaging and Signal Analysis*. Boston, MA: Artech House, 2002. 24, 32

[19] J. R. Guerci, *Space-Time Adaptive Processing for Radar*. Norwood, MA: Artech House, 2003. 28

[20] R. D. Chapman, C. Hawes, and M. E. Nord, "Target motion ambiguities in single-aperture synthetic aperture radar," *Aerospace and Electronic Systems, IEEE Transactions on*, vol. 46, no. 1, pp. 459–468, Jan 2010. 29, 36

[21] "Geforce gtx690 specifications," http://www.geforce.com/hardware/desktop-gpus/geforce-gtx-690/specifications, 2014, accessed: 15 Apr 2014. 41, 42

[22] "Shapefile," http://en.wikipedia.org/wiki/Shapefile, March 2014, accessed: 9 May 2014. 51

[23] "Calculate distance, bearing and more between latitude/longitude points," http://www.movable-type.co.uk/scripts/latlong.html, April 2014, accessed: 12 May 2014. 51

[24] "Two gpus, one insane graphics card: Introducing the geforce gtx titan z," http://blogs.nvidia.com/blog/2014/03/25/titan-z/, 2014, accessed: 3 May 2014. 53